Authors reply by Loeka Jongejans, on behalf of all authors (loeka.jongejans@awi.de)

We thank the referee for their constructive comments. We have revised our manuscript accordingly to your suggestions. Below, we addressed and replied to the suggestions that you made.

Referee Comment (RC): I completely agree with the authors that especially in remote arctic environments it is often not possible to use sampling schemes with a high number of replicates. And every data set we can get from these areas is worth the effort. Nevertheless, the issue of low representativity has to taken into account when discussing data or setting it into a larger context, for instance with respect to a whole Island.

Authors Reply (AR): Our work provides a first estimate of the OC pool size of the Baldwin Peninsula deposits. It is based on the data from the five study sites which correspond to the main landscape units in the study area: yedoma (30% of surface area), drained thermokarst lake basin (65%) and thermokarst lake deposits (5%). Furthermore, these three landscape units make up the largest share of the total yedoma permafrost region, where generally only a small part is covered by other sediments such as deltaic and fluvial sediments (Jorgenson et al., 2008; Romanovskii, 1993; Strauss et al., 2013). For this estimate we assumed homogeneity over the Baldwin Peninsula. In addition, bootstrapping the results helps constrain the standard error of the estimate. We are certain that further studies will help provide a better constrain on our estimate as more samples are added and spatial heterogeneity is addressed.

RC: With respect to the "volumetric OC" - unit weight over unit volume (which is also defined by an area e.g. sqm) is exactly OC stock, so here we seem to just have a case of different wording between soil science and paleo/geography.

AR: Thank you for the clarification.

RC: With respect to a phrase in the abstract: "importance of lipid biomarker analysis for determining the potential future greenhouse gas emissions from thawing permafrost" - here you definitely overrating lipid biomarkers. You should re-phrase these statements.
This also applies to the phrase "high quality" with respect to the lipid biomarkers. What is "high quality"? I guess you refer here to OM that has still the signature of the initial source material. I would be more specific here. For instance some studies refer to "low quality" OM with respect to sawdust or straw, materials that are definitely comparable to fresh arctic dwarf shrub or sedge vegetation. I would recommend being more specific here and refer to "unaltered OM" or comparable phrases.

AR: We thank you for the comment and rephrased the sentence in the abstract as suggested.
Indeed, quality refers to OM decomposability and high quality refers to well preserved material. We added a more detailed explanation in the introduction and made appropriate changes throughout the manuscript.

RC: With respect to the Conclusions I still think you could do better in terms of carving out the implications of your work, rather than just reporting your data.

AR: We made changes to the conclusion and added a sentence highlighting the implications of this study.

Organic ~~carbon~~ matter characteristics in yedoma and thermokarst deposits on Baldwin Peninsula, West-Alaska

Loeka L. Jongejans[1], Jens Strauss[1], Josefine Lenz[1,2], Francien Peterse[3], Kai Mangelsdorf[4], Matthias Fuchs[1,5] and Guido Grosse[1,5]

[1]Alfred Wegener Institute Helmholtz Centre for Polar and Marine Research, Permafrost Research Section, Potsdam, Germany
[2]University of Alaska Fairbanks, Institute of Northern Engineering, Fairbanks, USA
[3]Utrecht University, Department of Earth Sciences, Utrecht, Netherlands
[4]Helmholtz Centre Potsdam - German Research Centre for Geosciences, Germany
[5]University of Potsdam, Institute of Earth and Environmental Sciences, Potsdam, Germany

Correspondence to: Loeka L. Jongejans (loeka.jongejans@awi.de)

Abstract. As Arctic warming continues and permafrost thaws, more soil and sedimentary organic ~~carbon~~ matter (~~OC~~OM) will be decomposed in northern high latitudes. Still, uncertainties remain in the quality of the OM and the size of the organic carbon (OC) pools ~~quantity and quality of OC~~ stored in different deposit types of permafrost landscapes. This study presents ~~OC~~ OM data from deep permafrost and lake deposits on the Baldwin Peninsula which is located in the southern portion of the continuous permafrost zone in West-Alaska. Sediment samples from yedoma and drained thermokarst lake basin (DTLB) deposits as well as thermokarst lake sediments were analyzed for cryostratigraphical and biogeochemical parameters and their lipid biomarker composition to identify the belowground OC pool size and OM quality of ~~belowground OC pools in~~ ice-rich permafrost on Baldwin Peninsula. We provide the first detailed characterization of yedoma deposits on Baldwin Peninsula. We show that three quarters of soil organic carbon in the frozen deposits of the study region (total of 68 Mt) is stored in DTLB deposits (52 Mt) and one quarter in the frozen yedoma deposits (16 Mt). The lake sediments contain a relatively small OC pool (4 Mt), but have the highest volumetric OC content (93 kg m^{-3}) compared to the DTLB (35 kg m^{-3}) and yedoma deposits (8 kg m^{-3}), largely due to differences in the ground ice content. The biomarker analysis indicates that the ~~OC~~ OM in both yedoma and DTLB deposits is mainly of terrestrial origin. Nevertheless, the relatively high carbon preference index of plant leaf waxes in combination with a lack of degradation trend with depth in the yedoma deposits indicates that ~~OC~~ OM stored in yedoma is less degraded than that stored in DTLB deposits. This suggests that ~~OC~~ OM in yedoma has a higher potential for decomposition upon thaw, despite the relatively small size of this pool. These findings show that ~~highlight the importance of~~ the use of lipid biomarker analysis is valuable in the assessment of ~~for determining~~ the potential future greenhouse gas emissions from thawing permafrost, especially because this area close to the discontinuous permafrost boundary is projected to thaw substantially within the 21st century.

1 Introduction

The Arctic region is warming twice as fast as the global mean (Overland et al., 2017). Ice-rich permafrost soils are particularly vulnerable to climate warming and susceptible to large-scale thermokarst processes. Thermokarst is the subsidence of ground resulting from the thawing of ice-rich permafrost (Grosse et al., 2013; Günther et al., 2013). Thermokarst lake development often starts with the coalescence of polygonal ponds after the degradation of ice wedges (Grosse et al., 2013). This is followed by the formation of a body of unfrozen ground underneath the lake (i.e. talik) and subsequently, both the lake and talik grow and deepen. Thermokarst lake development can cease by drainage through lateral outflows formed by thermal erosion of ice wedge networks, by tapping of lakes due to coastal erosion, by vertical outflow through open taliks in regions with thin permafrost, or by infilling with sediment or encroaching vegetation (Burn and Smith, 1990; Jones and Arp, 2015; Lenz et al., 2016c). After lake loss, the remaining basins largely become vegetated and eventually permafrost can reform (Jones et al., 2012). Due to the different stages of lake development, thermokarst landscapes are highly dynamic and form complex patterns of landscape units (Jones et al., 2012; Lenz et al., 2016a).

Late Pleistocene, ice-rich syngenetic permafrost, known as yedoma, is especially prone to rapid and deep thaw processes (Schirrmeister et al., 2013). These deposits cover large regions of Siberia and Alaska (Kanevskiy et al., 2011; Schirrmeister et al., 2013; Strauss et al., 2017) and can reach a thickness of up to 50 m (Sher, 1997; Shur et al., 2012). Yedoma contains large syngenetic ice-wedges and can have a ground ice content of up to 80 vol%, thus yedoma deposits are highly vulnerable to thermokarst processes (Kanevskiy et al., 2016; Ulrich et al., 2014).

Permafrost landscapes store large quantities of OC (Hugelius et al., 2014; Strauss et al., 2013) as the generally low decomposition rates, due to low soil temperatures and poor drainage, inhibit decomposition of organic matter (Davidson and Janssens, 2006). Permafrost thaw and talik formation, however, allow microbial decomposition of the previously freeze-locked ~~OC~~OM, resulting in increased greenhouse gas emissions (in particular carbon dioxide and methane) into the atmosphere and enhancing the initial warming (Koven et al., 2015; Schuur et al., 2015; Strauss et al., 2017). Rapid and large-scale permafrost degradation of ice-rich permafrost, such as yedoma deposits, may constitute a positive feedback to atmospheric warming.

Due to the freezing conditions during and after accumulation, the ~~OC~~ OM stored in yedoma deposits is highly decomposable (Knoblauch et al., 2013; Schädel et al., 2014a; Strauss et al., 2017). Yedoma deposits contain on average less OC than DTLB deposits (e.g. Strauss et al., 2013), however higher respiration rates from yedoma deposits have been observed compared to DTLB deposits (Dutta et al., 2006; Lee et al., 2012; Zimov et al., 2006). Moreover, previous studies found that the state of ~~OC~~ OM decomposition is more dependent on ~~OC~~ OM properties, rather than on ~~OC~~ the age (Knoblauch et al., 2013; Stapel et al., 2016). It is therefore crucial to characterize the ~~quantity and~~ size of the ~~quality of~~ OC pools and the quality of the OM in both undisturbed as well as disturbed ice-rich permafrost landscapes, so that the potential contribution to future greenhouse gas release following permafrost degradation can be better constrained for each of the different landscapes.

Field Code Changed
Field Code Changed
Field Code Changed
Field Code Changed
Field Code Changed
Field Code Changed
Field Code Changed
Field Code Changed
Field Code Changed
Field Code Changed
Field Code Changed
Field Code Changed
Field Code Changed

This study aims to characterize the belowground ~~OC~~ OM stored in thermokarst affected areas by analyzing sediment samples from yedoma deposits, drained thermokarst lake basin deposits and thermokarst lake sediments. Two main questions are addressed: 1) how much OC is stored and 2) what is the quality of ~~this OC~~ the OM? We want to identify the OC pool size and the vulnerability. The latter depends on the state of decomposition (i.e. vulnerability to future decomposition), expressed as quality, where a high quality refers to well preserved material. ~~In this study, we particularly refer to belowground OC and the quality of OC refers to the decomposability of the material, respectively the vulnerability to future decomposition.~~ In our analysis, we focus on cryostratigraphical (bulk density, absolute ice content) and biogeochemical parameters (total organic carbon, total nitrogen, carbon-nitrogen ratio and stable carbon isotopes) to estimate the OC pool size of the yedoma, DTLB and thermokarst lake sediments. In addition, lipid plant and soil specific biomarkers (*n*-alkanes and brGDGTs, respectively) were used to determine the source and quality of the ~~OC~~ OM pool~~s~~.

2 Material and methods

2.1 Study area

The study sites are located on the western coast of the Baldwin Peninsula, which is surrounded by the Kotzebue Sound in Northwest Alaska (66°40' N, 162°15' W) (Figure 1). The Baldwin Peninsula is part of the former landmass Beringia that remained unglaciated during the Late Pleistocene (Hopkins, 1982). The peninsula is located in southern portion of the continuous permafrost zone and therefore close to the discontinuous permafrost boundary (Jorgenson et al., 2008). According to geological maps, the peninsula is largely composed of a sequence of marine, fluvial and glaciogenic sediments which are well exposed along coastal bluffs and in some regions covered by loess-like deposits (Hopkins et al., 1961; Huston et al., 1990; Pushkar et al., 1999). This study represents the first characterization of yedoma deposits on Baldwin Peninsula. A field campaign in summer 2016 revealed several yedoma exposures in active retrogressive thaw slumps on the western coast of the peninsula that consisted of fine-grained, ice-rich permafrost deposits penetrated by large syngenetic ice wedges. These yedoma exposures were located in upland remnants, a setting which is typical for yedoma hills found in northeast Siberia (Schirrmeister et al., 2013). A large portion of the peninsula has been affected by severe permafrost degradation and multiple thermokarst lake basin generations visible in satellite imagery (Figure 1). The present-day climate is subarctic with an average annual precipitation of 280 mm and a mean annual air temperature of -5.2°C (US Climate Data, 2017).

Field Code Changed

Field Code Changed

Field Code Changed

Field Code Changed

Field Code Changed

2.3 Field work

Sampling of yedoma and drained thermokarst lake basin (DTLB) exposures and thermokarst lake sediments was carried out on the western coast of the Baldwin Peninsula in August 2016 (Table 1). Photographs of the exposures and the lake core are shown in Supplement 2.1. The samples were named as follows: the geographical region (BAL for Baldwin Peninsula), the year of sampling (16 for 2016), the setting (B for bluff, UPL for upland), the site numbers (here: 2, 4) and the sampling of an aquatic environment was indicated (L for lake) (Table 1).

A yedoma coastal bluff (BAL16-B2) of 16 m thickness was sampled. This bluff is characterized by sediments containing large ice wedges, ice bands and ice lenses, which are overlying a separate unit of ice-rich silty sediments. Due to the difficult terrain and fast thawing of the deposits in summer, it was not possible to sample the whole exposure in one straight profile. Therefore, 25 samples of the yedoma deposits were collected using a handheld power drill (ø 57 mm) at five different sampling locations along the exposure, forming a composite profile. Three additional samples were taken from the separate depositional unit underlying the yedoma which was not as ice-rich and did not contain in-situ formed ice wedges. Exposures of DTLB deposits ranging in thickness from 3 to 8 m were sampled from three exposed profiles (BAL16-B3, BAL16-B4 and BAL16-B5). 31 samples were collected from the 8-m-high DTLB exposure BAL16-B4 consisting of mostly laminated sediments that contained various cryotextural and organic features (e.g. ice inclusions, lenses, organic matter inclusions). The DTLB exposures BAL16-B3 (9 samples) and BAL16-B5 (4 samples) were sampled to generate a broader sample base for the estimates of the DTLB OC pool (the results of the two DTLB additional profiles BAL16-B3 and BAL16-B5 are shown by depth in Supplement 2.3). All samples from the yedoma and DTLB exposures were kept frozen until laboratory analysis at Alfred Wegener Institute (AWI), Helmholtz Centre for Polar and Marine Research, in Potsdam.

In addition, a 34-cm-long sediment core (BAL16-UPL1-L1) was retrieved from a shallow thermokarst lake (1.35 m deep at coring site) with a N-W extent, a length of about 1,400 m and a width of 800 m. Unfrozen, slightly layered, clayey silty lake sediments were retrieved in a PVC tube (ø 60 mm) using a piston corer and were kept cool until sub-sampling (9 samples) and laboratory analysis.

2.4 Bulk physical properties

In the laboratory, the sediment samples were freeze-dried. The absolute ice content was derived from the weight difference of the frozen and dry samples after Eq. (1) and is expressed in weight percentage (wt%).

$$Absolute\ ice\ content\ [wt\%] = \frac{wet\ weight - dry\ weight}{wet\ weight} * 100 \quad (1)$$

For the frozen samples, the bulk density BD_1 was calculated following Eq. (2).

$$BD_1[10^3\ kg\ m^{-3}] = (\varphi - 1) * -\rho_s \quad (2)$$

where φ is porosity (fraction) and ρ_s is the mineral density in [10^3 kg m^{-3}]. The porosity is derived from the volumetric ratio of ice and dry sample whereby a constant ice density was assumed of 0.91*10^3 kg m^{-3} (at 0°C) (Lide, 1999). For the mineral density, the density of quartz of 2.65*10^3 kg m^{-3} was taken (Rowell, 1994).

Field Code Changed

Field Code Changed

For the unfrozen thermokarst lake sediments, BD_2 was calculated following Eq. (3). The volume of the sediment was corrected to account for the compression of the sediment during sampling. The volume of the excess water in the core tube after sampling was measured and included in the volume calculation of the core sediment.

$$BD_2[10^3\ kg\ m^{-3}] = \frac{dry\ weight}{volume} \quad (3)$$

where dry weight is given in [g] and volume in [cm^3], respectively in [10^3 kg] and [m^3].

2.5 Radiocarbon dating

Macrofossils of 15 samples were dated for accelerator mass spectrometry (AMS) radiocarbon dating in the Radiocarbon Laboratory in Poznan, Poland (Goslar et al., 2004). The radiocarbon ages were calibrated using the CALIB 7.1 software and the IntCal13 calibration curve (Stuiver et al., 2017). All calibrated ages are expressed as calibrated kilo years before present (cal ka BP), including the standard deviation (±). Infinite ages (>50,000 a) cannot be calibrated and hence, no uncertainty could be given.

2.6 Nitrogen and carbon content and composition

Homogenized samples were analyzed for total nitrogen (TN), total carbon (TC) and total organic carbon (TOC) using an elemental analyzer (Elementar Vario EL III and Elementar Vario Max C) and are expressed in [wt%]. The TOC/TN weight ratio was calculated and will be referred to as C/N. The stable carbon isotopic composition was determined by measuring $\delta^{13}C$ (ThermoFisher Scientific Delta-V-Advantage gas mass spectrometer equipped with a FLASH elemental analyzer EA 2000 and a CONFLO IV gas mixing system). The ratio is compared to the standardized Vienna Pee Dee Belemnite (VPDB) and expressed in per mille (‰ vs. VPDB). For samples with a TOC below the analytical accuracy (0.1 wt%), no C/N nor $\delta^{13}C$ was measured.

The combination of the C/N and $\delta^{13}C$ has been widely used as indicator of ~~OC~~ OM source. A higher C/N suggests an enhanced input of terrestrial land plants whereas algal produced matter is generally characterized by a lower C/N. The C/N and $\delta^{13}C$ ~~of OC~~ furthermore allow to distinguish between marine and lacustrine algae, where marine algae generally have a higher $\delta^{13}C$ (e.g. Lenz et al., 2016a; Meyers, 1994, 1997). Moreover, the C/N and $\delta^{13}C$ have been used as an indicator of ~~OC~~ OM decomposition, where a lower C/N and higher $\delta^{13}C$ indicate further degraded material (i.e. lower quality) (Gentsch et al., 2015; Gundelwein et al., 2007; Schädel et al., 2014b; Weiss et al., 2016a).

In order to compare the cryostratigraphy and biogeochemistry (BD, TOC, C/N and $\delta^{13}C$) of the three stratigraphical landscape units (yedoma, DTLB and thermokarst lake deposits), the non-parametric Kruskal-Wallis test and Mann-Whitney-Wilcoxon test were performed using the R statistical environment to test for significant differences. When the p-value exceeds 0.05, the null hypothesis (H_0: There is no statistically significant difference between the sample means of the different stratigraphic landscape units) cannot be rejected. In these statistical tests, the landscape units are treated separately and therefore, the internal differences of the study sites with depth and age are not included.

More extensive method descriptions of the elemental analysis can be found in Supplement 1.2.

2.7 Lipid biomarker analysis

2.7.1 Extraction and separation

Biomarker analysis was carried out to identify the ~~OC~~ OM composition and quality (Andersson and Meyers, 2012; Strauss et al., 2015). In total, 13 samples (6 from BAL16-B2 and 7 from BAL16-B4) were analyzed at the German Research

Field Code Changed
Field Code Changed
Field Code Changed
Field Code Changed
Field Code Changed

Centre for Geosciences (GFZ) for *n*-alkanes (long-chained, single bonded hydrocarbons) and branched glycerol diakyl glycerol tetraethers (brGDGTs; bacterial membrane lipids). The methods were adapted from Schulte et al. (2000) and Strauss et al. (2015). About 8 g of each sample was extracted (Dionex 200 ASE extractor) using dichloromethane/methanol (DCM/MeOH) (99:1 v/v) (heating phase 5 min, static phase 20 min at 75°C and 106 Pa). Excess solvent was evaporated under N_2. A known amount of four internal standards was added: 5α-androstane, ethylpyrene, 5α-androstan-17-on and erucic acid. The samples were passed over a sodium sulfate column with *n*-hexane prior to separation by medium-pressure liquid chromatography (MPLC) (Radke et al., 1980) into three fractions: aliphatic hydrocarbons, aromatic hydrocarbons and nitrogen-, sulfur-, and oxygen (NSO) containing compounds. The dissolved extracts were injected into the MPLC system where they were led through a column and pre-columns (thermally deactivated silica 100 63-200 µm and 200-500 µm on top with ratio ~7:1) with *n*-hexane. The NSO-fraction was further separated manually into a polar and acid fraction using a KOH-impregnated silica gel column with DCM.

Field Code Changed

Field Code Changed

Field Code Changed

2.7.2 Measurements

The *n*-alkanes were measured as part of the aliphatic fraction using gas chromatography (GC) - mass spectrometry (MS) (Trace GC Ultra and MS DSQ, Thermo Electron Corporation) using helium as a carrier gas. The samples were vaporized (50°C to 300°C with 10°C/s, 10 min isothermal holding) and led through a capillary column (BPX5; 22 mm x 50 m, film thickness 0.25 µm) (Peters et al., 2005). The oven was programmed from 50°C to 310°C (3°C/min and 30 min isothermal holding). The GC was linked to the MS to enable compound identification (ionization mode at 70 eV, 230°C). Full scan mass spectra were obtained from m/z 50 to 600 Da (2.5 scans/s). Using the software XCalibur, the peaks in the GC-MS total ion current chromatogram were integrated manually. The *n*-alkanes were quantified by comparing the peak area of the target compounds to the applied internal standards.

Field Code Changed

The brGDGTs were measured as part of the acid fraction using high-performance liquid chromatography (Shimadzu LC-10AD HPCL device coupled to a Finnigan TS 7000 mass spectrometer with APCI interface). The compounds were separated at 30°C over a Prevail Cyano column (2.1x150 mm, 3µm; Alltech) preceded by a precolumn filter of the same material, which does not separate 5- and 6-methyl isomers. Each fraction was eluted isocratically with *n*-hexane A and isopropanol B (5 min. 99% A and 1% B, linear gradient to 1.8% B within 40 min, in 1 min to 10% B holding for 5 min and back to initial conditions in 1 min, held for 16 min) with a flow rate of 0.2 mL/min. The APCI device has a corona current of 5 µA, voltage of 5 kV, the vaporizer temperature is 350°C and the capillary temperature 200°C. The source operates with nitrogen sheath gas at 60 psi without auxiliary gas. Full mass spectra were obtained at a scan rate of 0.33 s. The integration was performed in XCalibur and the quantification was performed by comparing the compound peaks to an Archaeol run.

2.7.3 Biomarker derived indices

The carbon preference index (CPI) of the *n*-alkanes was calculated after Marzi et al. (1993) following Eq. (4), and the average chain length (ACL) after Poynter and Eglinton (1990) following Eq. (5).

Field Code Changed

Field Code Changed

$$CPI_{23-33} = \frac{\sum_{i=n}^{m} C_{2i+1} + \sum_{i=n+1}^{m+1} C_{2i+1}}{2*(\sum_{i=n+1}^{m+1} C_{2i})} \quad (4)$$

where n is the starting dominating chain length divided by 2, m the ending dominating chain length divided by 2 and i the carbon number index.

$$ACL_{23-33} = \frac{\sum iC_i}{\sum C_i} \quad (5)$$

where i is the carbon number and C the concentration. For the calculation of both CPI and ACL, the interval of C_{23} to C_{33} was used. The ACL indicates ~~OC~~ OM source, where higher land plants (i.e. vascular plants) are dominated by long-chain *n*-alkanes of 25 to 30 carbon atoms, whereas bacteria and algae contain mainly shorter chains of 15 to 20 carbon atoms (Killops and Killops, 2013; Strauss et al., 2015). The CPI is the odd-to-even predominance of the hydrocarbons and indicates the degree of degradation of the ~~OC~~OM, where a lower value indicates further degraded material (Andersson and Meyers, 2012; Glombitza et al., 2009).

Field Code Changed

2.8 Landscape organic carbon pool estimation

A map of key landscape units (yedoma hills, DTLBs and thermokarst lakes) of the northern part of Baldwin Peninsula was developed in order to calculate the coverage for each landscape unit and to allow a first-order estimate of the belowground OC storage. Using a Landsat 8 satellite image (false color image with short-wave infrared, near-infrared and deep blue bands (bands 7-5-1), pixel resolution 30 m) as well as a digital terrain model (DTM; grid cell resolution 5 m), the three main landscape units were manually mapped and digitized for the northern part of the Baldwin Peninsula (~450 km^2). A similar approach of operator-driven thermokarst mapping by manually digitizing landforms from remote sensing imagery in combination with a DTM was successfully applied by Morgenstern et al. (2011) and Farquharson et al. (2016).

Field Code Changed

Field Code Changed

The total OC pool on Baldwin Peninsula was then estimated based on the deposit thickness, the spatial coverage, wedge ice volume (WIV), BD and TOC from the sampled exposures and cores (BAL16-B2 to B5 and BAL16-UPL1-L1) following Eq. (6).

$$Total\ OC\ pool\ [Mt] = \frac{thickness * coverage * \frac{100-WIV}{WIV} * BD * \frac{TOC}{100}}{10^6} \quad (6)$$

where the deposit thickness is given in [m], spatial coverage in [m^2], WIV in [vol%], BD in [10^3 kg m^{-3}] and TOC in [wt%]. The deposit thickness is based on few field observations and for this first-order assessment assumed constant over the whole peninsula. Deeper deposits below frozen yedoma and DTLB are excluded due to unknown spatial coverage and thickness. Also, the deposits below lake sediments, potentially unfrozen in a talik, are not included in the calculation. The spatial coverage per landscape unit was calculated from the land coverage classification map. Strauss et al. (2013) calculated the average WIV for yedoma and DTLB deposits based on polygon size and ice-wedge width and depth. WIV was assumed to be zero for the thermokarst lake sediments. In order to compensate for possibly non-continuous field sampling, weighted BD*TOC values over depth were used by value replication depending on depth interval. The data were extrapolated to the northern part of the Baldwin Peninsula (i.e. the mapped part). The volumetric OC pool was estimated according to Eq. (7).

$$Volumetric\ OC\ pool\ [kg\ m^{-3}] = \left(\frac{100-WIV}{WIV} * BD * \frac{TOC}{100}\right) * 10^3 \quad (7)$$

The calculation for each landscape unit was performed separately using bootstrapping techniques, which included 10^4 iterations of random sampling with replacement, after which the mean and standard deviation were calculated. Because BD and TOC are correlated, paired values were used during the random sampling.

3 Results

3.1 Biogeochemical and biomarker proxies

3.1.1 Yedoma exposure

Radiocarbon dates for yedoma exposure BAL16-B2 range from >50,000 to 10,000 cal a BP (Table 2). There is no consistent age-depth relationship: while a few samples, including the near-surface sample, have an infinite age, the second youngest sample is found at a depth of 1600 cm. The cryostratigraphical and biogeochemical parameters are presented by depth (Figure 2). Depths are measured from the cliff top downwards for the yedoma and DTLB exposures, and from the sediment surface downwards for the thermokarst lake sediments. The BD of the yedoma deposits (mean: 0.80*10^3 kg m^{-3}, sd: 0.18) shows most variation in the bottom part up to 1117 cm. The TOC ranges between 0.1 and 4.7 wt% (mean: 1.9 wt%, sd: 1.1). The C/N varies between 4.4 and 14.0 (mean: 10.1, sd: 2.9) and does not show a trend with depth. The $\delta^{13}C$ is in the range of -24.8 to -28.3 ‰ (mean: -25.9 ‰, sd: 0.9) and shows most variation up to 1080 cm. Exposure BAL16-B2 is very ice-rich with an average absolute ice content of 45 wt% (70 vol%).

The biomarkers concentrations and index values are presented by depth in Figure 3. The *n*-alkane concentration in the yedoma deposits ranges from 0.5 to 1.8 mg g^{-1} TOC (mean: 1.0 mg g^{-1} TOC, sd: 0.5). The $ACL_{23\text{-}33}$ varies between 28.8 in the bottom sample and 28.2 in the top with a peak of 30.0 at 1117 cm (mean: 28.8, sd: 0.6). The samples are dominated by *n*-alkane chains with a high number of carbon atoms: the dominating chains are *n*-C_{29} and *n*-C_{31} (Figure S7). The $CPI_{23\text{-}33}$ is in the range of 9.0 to 13.6 (mean: 11.6, sd: 2.0) and does not show a trend over depth. The sample at 1399 cm has the maximum brGDGT concentration of 1.3 µg g^{-1} TOC whereas the other samples have relatively low concentrations (mean: 0.5 µg g^{-1} TOC, sd: 0.5).

3.1.2 DTLB exposure

Radiocarbon ages for DTLB exposure BAL16-B4 (Table 2) are in the range from >50,000 cal a BP (788 to 434 cm) to 240 cal a BP (22 cm) and show no age inversions: the lower samples are of infinite age and the near-surface sediments are the youngest and show Holocene ages. The BD decreases upwards in the profile and ranges between 1.27 and 0.29*10^3 kg m^{-3} (mean: 0.91*10^3 kg m^{-3}, sd: 0.3), a particularly strong decrease occurs from 280 cm to 215 cm (Figure 2). The TOC (mean: 6.6 wt%, sd: 9.4) is higher in the interval from 250 to 22 cm than in the lower part, and strongly increases in the top 8 cm. The C/N increases towards the top, ranging from 11.3 at the bottom to 29.0 at the top (mean: 14.9, sd: 4.2). The $\delta^{13}C$ displays an

opposite trend with higher values in the lower part (-25.8‰) and a decrease near the surface (-28.7‰) (mean: -27.2‰, sd: 0.7), and a sudden decrease at 280 to 250 cm. The exposure has an average absolute ice content of 41 wt% (67 vol%).

The *n*-alkane concentration reaches its maximum of 16.0 mg g^{-1} TOC in the bottom sample whereas the other samples have much lower concentrations (mean: 4.3 mg g^{-1} TOC, sd: 5.4) (Figure 3). The ACL_{23-33} is higher than 28 for all samples except at 583 cm and 430 cm (mean: 28.3, sd: 0.4). The dominating *n*-alkane chains are *n*-C_{27} and *n*-C_{31} (Figure S7). The CPI_{23-33} increases towards the top from 5.7 to 12.6 (mean: 8.8, sd: 2.1). The brGDGT concentration varies between 0 and 3.8 µg g^{-1} TOC with the peak at 160 cm below the surface (mean: 1.5 µg g^{-1} TOC, sd: 1.4).

3.1.3 Thermokarst lake sediments

The radiocarbon age of the thermokarst lake core BAL16-UPL1-L1 (Table 2) is 2,010 cal a BP at a depth of 26.5-27.5 cm and 480 cal a BP at 19-20 cm. The sedimentological and biogeochemical parameters (Figure 2) have a low variability along the core profile with a mean for BD of 0.78*10^3 kg m^{-3} (sd: 0.01), TOC of 14.4 wt% (sd: 0.5), C/N of 22.5 (sd: 0.6) and $\delta^{13}C$ of -28.5 ‰ (sd: 0.2). The $\delta^{13}C$ shows a slight decrease towards the lake sediment surface.

3.1.4 Statistical significance

We found significant differences ($p<0.05$) for all (pairwise) comparisons of the biogeochemical parameters between the yedoma, DTLB and thermokarst lake deposits on Baldwin Peninsula (Supplement 2.6). The DTLB deposits have the highest BD and the thermokarst lake sediments the lowest. The TOC and C/N are highest in the thermokarst lake sediments followed by the DTLB and then the yedoma deposits, whereas the $\delta^{13}C$ shows an opposite trend.

3.2 Organic carbon pool estimation

We produced a land cover classification map distinguishing between yedoma, DTLBs, thermokarst lakes and lagoons (Figure 4). For the lakes on yedoma uplands and lagoons, no field information is available, so that those areas are excluded from further OC pool calculations. The total area mapped is about 450 km^2 of which ~65% is covered by DTLB, ~30% by yedoma and ~5% by thermokarst lakes (Table 3). The input parameters of the bootstrapping for the OC pool estimates are shown in Table 3. The volumetric and total OC pool per stratigraphic landscape unit for the frozen deposits and unfrozen thermokarst lake sediments are presented in Table 3, where the WIV is included. The OC pool estimates without WIV are also reported to allow comparison with other studies (Table 3). The yedoma deposits contain 8.0±0.8 kg OC m^{-3} (15.3±1.6 excl. WIV) and the DTLB deposits 34.7±2.9 kg OC m^{-3} (37.4±3.1 excl. WIV), which corresponds to a total OC pool of 16.3±1.7 Mt (31.4±3.3 excl. WIV) in yedoma and 51.5±4.3 Mt (55.4±4.6 excl. WIV) in DTLB deposits. The total estimate of the total OC pool of the frozen sediments on northern Baldwin Peninsula is ~68 Mt OC. The thermokarst lake sediments contain 92.9±0.8 kg OC m^{-3} which adds up to a total pool of 3.9±0.0 Mt for all thermokarst lakes in the study area.

4 Discussion

4.1 Landscape development and carbon dynamics

4.1.1 Sediment facies

The yedoma deposits of BAL16-B2 have ~~been~~ accumulated in a stable predominantly aeolian depositional environment, as shown by the grain size distribution (detailed method description and results of the grain size analysis are given in Supplement 1.1 and 2.5.1). The grain size distributions indicate that these deposits are characterized by a stronger aeolian influence than northeastern Siberian yedoma sites (Schirrmeister et al., 2008b; Strauss et al., 2012). Field observations suggest that the lower part of exposure BAL16-B2 (1,600 to 1,870 cm) is a separate unit. The significant change in sediment type from very coarse silt to medium silt (p-value<0.05), reflected in the grain size distributions (Supplement 2.5.1), confirms this distinction.

The formation of yedoma deposits on the west coast of the Baldwin Peninsula at study site BAL16-B2 possibly started before 50 cal ka BP. The large range of radiocarbon ages in these yedoma deposits suggests that they are mixed with ancient or younger organic material. According to Vasil'chuk and Vasil'chuk (2017), contamination with ancient organic material is common in yedoma deposits, due to the syngenetic character of the deposits. Therefore, they proposed to take the youngest age of the sediments, justified by the fact that age rejuvenation is not likely, due to the undisturbed character of the deposits. However, it is unlikely that relatively young sediments (~17 cal ka BP at 1600 cm) are overlain by a few meters of older sediments (~45 cal ka BP at 1117 cm and infinite ages at 1399 and 1500 cm), suggesting that the young ages could be the result of re-deposition. Considering that BAL16-B2 is a coastal bluff, re-deposition of young material cannot be neglected. Furthermore, the ages fall in the range of previous studies from Siberian yedoma deposits (> 57 to 13 ka BP) (Schirrmeister et al., 2002a, 2002b, 2003; Strauss et al., 2013) and Alaskan yedoma deposits (> 48 to 14 ka BP) (Kanevskiy et al., 2011), except for the sample at 945 cm (~10 cal ka BP). Generally, care should be taken with the interpretation of dating of yedoma deposits.

The lower part of the DTLB exposure BAL16-B4 has a radiocarbon age of 46 cal ka BP or older, which suggests that the lowest deposits have been accumulated during the same time as yedoma formation. However, the TOC and C/N are significantly lower in BAL16-B2 than in BAL16-B4 whereas the $\delta^{13}C$ is significantly higher (Supplement 2.6). This suggests that the DTLB deposits are a mixture of former yedoma deposits thawed and partially decomposed in a lake talik, lake sediments and post-drainage terrestrial peat. The grain size signal for both exposures is very similar (p>0.05), suggesting a connection between the BAL16-B2 and BAL16-B4 sediments, which can be explained by the Holocene reworking of the yedoma sediments in the lake and in the talik affected by subsidence. The branched and isoprenoid tetraethers (BIT) index (detailed method description and results of the biomarker climatic indicator are given in Supplement 1.3 and 2.5.2) is lower for BAL16-B2 than for BAL16-B4, which may indicate that the sediments in BAL16-B2 have been deposited in a drier climate (Dirghangi et al., 2013), in line with earlier paleoenvironmental reconstructions (e.g. Andreev et al., 2011; Lenz et al., 2016c).

In exposure BAL16-B4 a change was observed in the proxy records (age, BD, TOC, $\delta^{13}C$) between 280 and 250 cm: the sediments above 250 cm have lower BD and $\delta^{13}C$ and a higher TOC and C/N compared to the sediments below 280 cm. Furthermore, there is a change in sediment type, as shown by the different grain size distributions below 280 and above 250 cm

Field Code Changed

Field Code Changed

Field Code Changed

Field Code Changed

Field Code Changed

(Supplement 2.5.1), and in the depositional environment, as shown by a change in the relative brGDGT distribution, reflected in the methylation of branched tetraethers (MBT) index (Supplement 1.3 and 2.5.2). These changes suggest the initiation of a thermokarst lake: the sediments below 280 cm likely are former yedoma sediments that were thawed in situ in a talik (taberite), whereas the upper sediments are lake sediments. The lake initiation likely happened during the Holocene. The drainage of the lake is not recorded in the data; the drainage event took place after 2.08 cal ka BP.

The thermokarst lake sediments from BAL16-UPL1-L1 have been accumulated during the Holocene (2,010 and 480 a BP). Assuming a recent age for the surface sediments, the calculated sedimentation rate between 2,010 and 480 years BP was ~6 cm ka^{-1} and the sedimentation rate for the last 480 years ~50 cm ka^{-1}. For comparison, Lenz et al. (2016b) found a mean sedimentation rate for Peatball Lake, Alaska, of ~70 cm ka^{-1} for the last 1,400 years. The BD, TOC, C/N and $\delta^{13}C$ of the sediment core BAL16-UPL1-L1 show minimal variation, suggesting a stable depositional environment. Therefore, a hiatus in the sediment is unlikely.

Field Code Changed

4.1.2 Organic carbon quantity

To estimate future release of greenhouse gases from permafrost soils, the thaw-vulnerable OC pool needs to be identified. The organic carbon quantity is identified by analyzing the TOC and estimating the OC budget. The thermokarst lake sediments have the highest TOC of the three landscape units, which is likely due to the addition of organic matter from lake primary production, as well as the integration of organic matter from its catchment. The DTLB deposits cover a large range of TOC values, which corroborates the findings from section 4.1.1 that the deposits are a mixture of reworked and new material. The TOC content of the yedoma deposits is comparable to TOC values reported in previous yedoma studies from across Siberia and Alaska (Figure S6) (Schirrmeister et al., 2008a, 2008b, 2011; Strauss et al., 2012, 2013, 2015). Although the mean TOC content of the yedoma deposits is relatively low compared to that of DTLB deposits and thermokarst lake sediments, the volume of the yedoma deposits is of importance for the OC pool size, due to the large spatial coverage and thickness deposits.

The thermokarst lake sediments (~93 kg m^{-3}) have the highest volumetric OC pool compared to the yedoma and DTLB deposits. The DLTB deposits (~35 kg m^{-3}) contain four times as much OC by volume as yedoma deposits (~8 kg m^{-3}) and more than two times as much (DTLB: ~37 kg m^{-3}, yedoma: ~15) when excluding WIV. Multiple studies have been carried out to estimate OC pool size of deep yedoma and DTLB deposits. Here, we compare the volumetric OC pool to that of other studies excluding WIV, to compare the OC content of the frozen sediment only. Zimov et al. (2006) found that yedoma deposits contain on average 18.5 kg m^{-3} which is comparable to the yedoma deposits of Baldwin Peninsula. Furthermore, the DTLB OC pool of Baldwin Peninsula is in the range of 35.5 to 86.2 kg soil OC m^{-3} that Mueller et al. (2015) estimated for DTLB deposits in the Alaskan north slope region. Schirrmeister et al (2011) (Northeast Siberia) (DTLB: 53.5, yedoma: 21.1-33.2 kg m^{-3}) and Strauss et al. (2013) (total yedoma region, ~1,387,000 km^2) (DTLB: ~33, yedoma: ~19 kg m^{-3}) both estimated the OC budget of deep permafrost deposits (25 m deep) and found that DTLB deposits contain 1.5 to 2 times as much OC as yedoma deposits. Shmelev et al. (2017) found a slightly higher volumetric OC budget for thermokarst deposits (14.2 kg m^{-3}) than for yedoma deposits (12.6 kg m^{-3}).

Field Code Changed
Field Code Changed
Field Code Changed
Field Code Changed

On the other hand, Webb et al. (2017) also estimated the OC pool of Siberian deep deposits (0-15 m) and found that the yedoma deposits contained more OC (7.9 to 21.6 kg m^{-3}) than the DTLB deposits (6.9 to 14.5 kg m^{-3}). Other studies in Siberia (Fuchs et al., 2018; Siewert et al., 2016) also found more OC stored in yedoma deposits than in DTLB deposits. However, the estimates of these studies were based on near-surface sediments (0-2 m).

Based on our landscape unit map we scaled the total OC pool of the Baldwin Peninsula. About 70% of the area of Baldwin Peninsula is affected by permafrost degradation (e.g. thermokarst processes or coastal erosion) and is therefore classified as thermokarst. Moreover, these thermokarst processes led to more than 10 m of ground subsidence on the Baldwin Peninsula, as suggested by relief differences between yedoma uplands and DTLB. The estimated OC pool of the frozen sediments (yedoma 0-15 m depth, DTLB 0-5 m depth) on Baldwin Peninsula is ~68 Mt, of which roughly three quarters (~52 Mt) is stored in DTLB deposits and one quarter (~16 Mt) in yedoma deposits. This high amount of OC stored in an area of approximately 450 km^2 shows the important contribution of these deep thermokarst affected yedoma deposits to pan-arctic soil organic carbon stock estimations.

4.2 Organic ~~carbon~~ matter quality

Permafrost conditions limit decomposition of ~~OC~~OM, thereby preserving the quality ~~of the OC~~. The ~~OC~~ OM quality is identified by analyzing the OM~~OC~~ composition of the sediments. The source of OM~~OC~~ influences both the quantity as well as the quality of OM~~OC~~. The ACL_{23-33} for both the yedoma (>28.2) and DTLB (>27.7) deposits suggests that the organic matter is mainly derived from terrestrial higher plants. Additionally, in all samples, the long- and odd-chains dominate, which is also typical for a terrestrial higher plant origin (Eglinton and Hamilton, 1967).

Figure 5 shows a scatter plot of the C/N and $\delta^{13}C$ for the three landscape units of this study and other studies from Alaska: yedoma deposits along the Itkillik River (Lapointe et al., 2017; Strauss et al., 2012), DTLB deposits from the Northern Seward Peninsula (Lenz et al., 2016c) and thermokarst lake sediments from lakes in the Kobuk River Delta and Central Seward Peninsula (Lenz et al., 2018). We found significant statistical differences ($p<0.05$) in almost all tests attempting to differentiate between OM~~OC~~ composition in yedoma, DTLB and thermokarst lake deposits of the Baldwin Peninsula and the other Alaskan studies based on the C/N and the $\delta^{13}C$ (Supplement 2.6). A trend exists from a low C/N and high $\delta^{13}C$ in yedoma deposits towards a high C/N and low $\delta^{13}C$ in the thermokarst lake sediments (Figure 5). Intermediate C/N and $\delta^{13}C$ were found for DTLB deposits. The high $\delta^{13}C$ and low C/N for the yedoma exposure (BAL16-B2) is typical (Dutta et al., 2006; Sánchez-García et al., 2014; Vonk et al., 2013), since it is characteristic for stadial periods with decreased productivity and a dry climate (Schirrmeister et al., 2011, 2013). The C/N and $\delta^{13}C$ of the DTLB deposits show a large range, which reflects the mixed character of the disturbed landscape: these deposits contain on the one hand reworked OM~~OC~~ (e.g. from former yedoma deposits) and on the other hand fresh OM~~OC~~ (e.g. from thermokarst lake production). ~~OC in t~~Thermokarst lake sediments ~~is~~

Field Code Changed
Field Code Changed
Field Code Changed
Field Code Changed
Field Code Changed
Field Code Changed
Field Code Changed

are generally characterized by a low $\delta^{13}C$ (Cohen, 2003; Meyers, 1994), which is also the case here (Figure 5). The high C/N of the thermokarst lake sediments likely is an indication that the OM~~OC~~ is of high quality due to contribution of fresh ~~OC~~ OM (Schirrmeister et al., 2013; Strauss et al., 2015). Hence, the trends of the C/N and $\delta^{13}C$ (Figure 5) between the landscape units can be explained mainly by the source of the OM~~OC~~.

Comparing the properties of the ~~OC~~ OM pools per landscape unit at Baldwin Peninsula with the Alaskan study sites in Figure 5 shows that the yedoma from Baldwin Peninsula does not have a significantly different C/N or $\delta^{13}C$ than that at Itkillik River ($p>0.05$; Supplement 2.6) which suggests that the OM~~OC~~ in both yedoma deposits has a similar composition. The DTLB deposits of Baldwin Peninsula have a significantly higher C/N ($p<0.01$) compared to Northern Seward Peninsula, but a similar $\delta^{13}C$ ($p>0.05$). The lower C/N at Northern Seward Peninsula can be explained by the multiple lake generations this basin went through, leading to generally more degraded OM~~OC~~ (Lenz et al., 2016a). Given that the C/N and $\delta^{13}C$ among thermokarst lakes at Baldwin Peninsula and Central Seward Peninsula are significantly indistinguishable ($p>0.05$), we argue that general contributions of lake production and thawed sediments from below are comparable, resulting in a similar OM~~OC~~ composition. The thermokarst lake in Kobuk River Delta, however, is significantly different in both proxies compared to Baldwin Peninsula and Central Seward Peninsula ($p<0.01$). The lower $\delta^{13}C$ at the Kobuk River Delta can be an indication that the lacustrine contribution ~~to the OC pool~~ is higher than in Baldwin Peninsula and Central Seward Peninsula. Nonetheless, the thermokarst lake sediments from Baldwin Peninsula, Kobuk River Delta and Central Seward Peninsula all have a relatively high C/N and low $\delta^{13}C$, compared to the yedoma and DTLB deposits (Figure 5). The similar composition of the two yedoma study sites suggests a lack of decomposition, thereby implying the undisturbed character of the deposits. Furthermore, the differences of the DTLB study sites are likely caused by further OM~~OC~~ composition in the Northern Seward Peninsula basin which could have occurred during multiple lake generations the basin went through. These findings suggest that the range of the C/N and $\delta^{13}C$ within the study sites can be explained mainly by the quality of the OM~~OC~~.

A significantly higher $CPI_{23\text{-}33}$ in yedoma compared to DTLB deposits (p-value<0.05) indicates that the OM~~OC~~ in the yedoma deposits is less degraded and, therefore, suggests that this pool has a higher potential for future ~~OC~~ decomposition. Furthermore, the decreasing trend in $CPI_{23\text{-}33}$ in the DTLB deposits indicates progressive degradation with depth, whereas the lack of such a trend in the yedoma deposits indicates that minimal or no decomposition has occurred before or after the organic matter was incorporated into the permafrost, maintaining its high quality (Stapel et al., 2016; Strauss et al., 2015; Weiss et al., 2016). These findings suggest that the ~~OC~~ OM in yedoma deposits BAL16-B2 is of higher quality than that in the DTLB deposits BAL16-B4. Previous studies reported relatively high carbon turnover rates of Alaskan yedoma deposits (Dutta et al., 2006; Lee et al., 2012; Zimov et al., 2006), which suggest the presence of easily degradable organic matter in these deposits, which corroborates our findings.

Schuur et al. (2009) showed that in thermokarst affected permafrost soils, old ~~OC~~ OM is released more strongly. Also, it was shown that the formation of mineral-organic associations can be an important factor influencing bioavailability of ~~OC~~ OM in permafrost soils, because it can improve the stability of OM~~OC~~ in soils (Gentsch et al., 2015; Gundelwein et al., 2007; Höfle et al., 2013). Vonk et al. (2010) also showed the presence of this altered mineral bound organic matter component in

Field Code Changed
Field Code Changed
Field Code Changed
Field Code Changed
Field Code Changed
Field Code Changed
Field Code Changed

Arctic river and marine sediments. However, it is not clear yet how large the share of mineral-associated organic matter in permafrost soils is and how it exactly influences the stability in high-latitude soils (Höfle et al., 2013; Mueller et al., 2015).

Regardless, to evaluate implications of permafrost degradation arising from future climate change, it is necessary to assess the vulnerability of the total OM~~O~~C pool. Climate change will increase the frequency and intensity of fires and floods which can lead to soil removal and disturbances of the ground thermal regime which can result in rapid local permafrost degradation (Grosse et al., 2011). Because of the high ice content in the yedoma and DTLB deposits on Baldwin Peninsula (>45 vol%, excluding WIV), the deposits are highly susceptible and vulnerable to deep permafrost thaw which will have a great effect on the topography. Lindgren et al. (2016) found a net increase in total lake surface area by 3.9% for the Baldwin Peninsula between 1972 and 2014. With the formation of new, deep lakes, primary productivity is expected to increase on a large scale, which will possibly compensate for increased greenhouse emissions initially. However, following the positive permafrost feedback loop, more intensive permafrost degradation will likely lead to an increase of the number of lake drainage events in West-Alaska (Lindgren et al., 2016). This could lead to rapid OM~~O~~C sequestration in new permafrost aggrading in DTLBs and evolving terrestrial peat, but will be followed by ultimate decomposition once this region, which is ~80 km from the discontinuous permafrost boundary (Brown et al., 1997), is affected by widespread permafrost near-surface thaw between 2050 and 2100 (Lawrence and Slater, 2005; Walter Anthony et al., 2014). Although the largest share of OC in frozen deposits on Baldwin Peninsula is stored in DTLB deposits (~75%), we showed that the OM~~O~~C in yedoma deposits is ~~of~~ better preserved ~~higher quality~~ and therefore, the OM~~O~~C in the yedoma is especially vulnerable to future microbial degradation and greenhouse gas release which will further enhance climate warming.

Field Code Changed
Field Code Changed
Field Code Changed
Field Code Changed
Field Code Changed
Field Code Changed

5 Conclusion

This study presents OM~~O~~C characteristics from ice-rich ~~permafrost~~ yedoma and DTLB deposits and thermokarst lake sediments on the Baldwin Peninsula, West-Alaska. We provide the first approximation of the size of the OC pools in ice-rich permafrost and the OM quality. ~~U~~using cryostratigraphical, biogeochemical and biomarker parameters ~~of yedoma deposits and DTLB deposits as well as thermokarst lake sediments, the size and quality of OC pools in ice-rich permafrost were identified.~~ The ~~first estimate of the~~ OC pool size of the frozen deposits ~~in a 450 km² study on the Baldwin Peninsula~~ is ~68 Mt for the 450 km^2 study area of the Baldwin Peninsula.~~,~~ Frozen DTLB deposits make up 75% of the total OC pool. ~~of which three quarters are stored in frozen DTLB deposits.~~ The biomarker distributions showed mainly terrestrial origin of the OM in both the yedoma and DTLB deposits. The lake sediments had the highest volumetric OC content of ~93 kg OC m^{-3} compared to yedoma (~8 kg OC m^{-3}) and DTLB deposits (~35 kg OC m^{-3}). Biogeochemical and biomarker parameters indicated that the OM~~O~~C in the yedoma deposits is best preserved and of higher quality than the OM~~O~~C stored in DTLB deposits and thermokarst lake sediments.~~,~~ Thus, yedoma deposits have ~~demonstrating the~~ higher potential for OM~~O~~C decomposition ~~in yedoma deposits~~, even though they make up only 25% of the OC pool. Ongoing climate change will lead to the formation of

deep thaw features and disturbances in yedoma permafrost. The rapid decomposition of the highly decomposable OM may potentially lead to significant greenhouse gas emissions.

Data publishing

The data presented in this study is available on PANGAEA (Jongejans et al., 2018).

Field Code Changed

Acknowledgements

This study was carried out within the ERC PETA-CARB project (#338335) and additional support by the Helmholtz Impulse and Networking Fund (#ERC-0013). L.L. Jongejans was financially supported through an Erasmus+ EU grant. Field work was carried out by the Alfred Wegener Institute, Helmholtz Centre for Polar and Marine Research and the U.S. Geological Survey (USGS). We thank the Kotzebue Community, Ben Jones (USGS), Jim Kincaid (Northwestern Aviation), Jim Webster (Webster's Flying Service) and Ingmar Nitze (AWI) for help in the field, and Dyke Scheidemann (AWI), Anke Sobotta and Cornelia Karger (German Research Centre for Geosciences) for their analytical support in the lab. We thank the editor and the anonymous referees for their helpful feedback.

References

Andersson, R. A. and Meyers, P. A.: Effect of climate change on delivery and degradation of lipid biomarkers in a Holocene peat sequence in the Eastern European Russian Arctic, Org. Geochem., 53(Supplement C), 63–72, doi:https://doi.org/10.1016/j.orggeochem.2012.05.002, 2012.

Andreev, A. A., Schirrmeister, L., Tarasov, P. E., Ganopolski, A., Brovkin, V., Siegert, C., Wetterich, S. and Hubberten, H.-W.: Vegetation and climate history in the Laptev Sea region (Arctic Siberia) during Late Quaternary inferred from pollen records, Quat. Sci. Rev., 30(17), 2182–2199, doi:https://doi.org/10.1016/j.quascirev.2010.12.026, 2011.

Brown, J., Ferrians Jr, O., Heginbottom, J. and Melnikov, E.: Circum-Arctic map of permafrost and ground-ice conditions, US Geological Survey Reston., 1997.

Burn, C. R. and Smith, M. W.: Development of thermokarst lakes during the holocene at sites near Mayo, Yukon territory, Permafr. Periglac. Process., 1(2), 161–175, doi:10.1002/ppp.3430010207, 1990.

Cohen, A. S.: Paleolimnology : the history and evolution of lake systems, Oxford Univ. Press, Oxford., 2003.

Davidson, E. A. and Janssens, I. A.: Temperature sensitivity of soil carbon decomposition and feedbacks to climate change, Nature, 440, 165, doi:10.1038/nature04514, 2006.

Dirghangi, S. S., Pagani, M., Hren, M. T. and Tipple, B. J.: Distribution of glycerol dialkyl glycerol tetraethers in soils from two environmental transects in the USA, Org. Geochem., 59, 49–60, doi:10.1016/j.orggeochem.2013.03.009, 2013.

Dutta, K., Schuur, E. A. G., Neff, J. C. and Zimov, S. A.: Potential carbon release from permafrost soils of Northeastern Siberia, Glob. Change Biol., 12(12), 2336–2351, doi:10.1111/j.1365-2486.2006.01259.x, 2006.

Eglinton, G. and Hamilton, R. J.: Leaf Epicuticular Waxes, Science, 156(3780), 1322–1335, doi:10.1126/science.156.3780.1322, 1967.

Farquharson, L., Anthony, K. W., Bigelow, N., Edwards, M. and Grosse, G.: Facies analysis of yedoma thermokarst lakes on the northern Seward Peninsula, Alaska, Sediment. Geol., 340, 25–37, doi:https://doi.org/10.1016/j.sedgeo.2016.01.002, 2016.

Fuchs, M., Grosse, G., Strauss, J., Günther, F., Grigoriev, M., Maximov, G. M. and Hugelius, G.: Carbon and nitrogen pools in thermokarst-affected permafrost landscapes in Arctic Siberia, Biogeosciences, 15(3), 953–971, doi:10.5194/bg-15-953-2018, 2018.

Gentsch, N., Mikutta, R., Shibistova, O., Wild, B., Schnecker, J., Richter, A., Urich, T., Gittel, A., Šantrůčková, H., Barta, J. and others: Properties and bioavailability of particulate and mineral-associated organic matter in Arctic permafrost soils, Lower Kolyma Region, Russia, Eur. J. Soil Sci., 66(4), 722–734, 2015.

Glombitza, C., Mangelsdorf, K. and Horsfield, B.: Maturation related changes in the distribution of ester bound fatty acids and alcohols in a coal series from the New Zealand Coal Band covering diagenetic to catagenetic coalification levels, Org. Geochem., 40(10), 1063–1073, doi:https://doi.org/10.1016/j.orggeochem.2009.07.008, 2009.

Goslar, T., Czernik, J. and Goslar, E.: Low-energy 14C AMS in Poznań Radiocarbon Laboratory, Poland, Nucl. Instrum. Methods Phys. Res. Sect. B Beam Interact. Mater. At., 223–224, 5–11, doi:https://doi.org/10.1016/j.nimb.2004.04.005, 2004.

Grosse, G., Romanovsky, V., Jorgenson, T., Anthony, K. W., Brown, J. and Overduin, P. P.: Vulnerability and Feedbacks of Permafrost to Climate Change, Eos Trans. Am. Geophys. Union, 92(9), 73–74, doi:10.1029/2011EO090001, 2011.

Grosse, G., Jones, B. and Arp, C.: 8.21 Thermokarst Lakes, Drainage, and Drained Basins, 2013.

Gundelwein, A., Müller-Lupp, T., Sommerkorn, M., Haupt, E. T. K., Pfeiffer, E.-M. and Wiechmann, H.: Carbon in tundra soils in the Lake Labaz region of arctic Siberia, Eur. J. Soil Sci., 58(5), 1164–1174, doi:10.1111/j.1365-2389.2007.00908.x, 2007.

Günther, F., Overduin, P. P., Sandakov, A. V., Grosse, G. and Grigoriev, M. N.: Short- and long-term thermo-erosion of ice-rich permafrost coasts in the Laptev Sea region, Biogeosciences, 10(6), 4297–4318, doi:10.5194/bg-10-4297-2013, 2013.

Höfle, S., Rethemeyer, J., Mueller, C. W. and John, S.: Organic matter composition and stabilization in a polygonal tundra soil of the Lena Delta, Biogeosciences, 10(5), 3145–3158, doi:10.5194/bg-10-3145-2013, 2013.

Hopkins, D. M.: Aspects of the paleogeography of Beringia during the Late Pleistocene, in Paleoecology of Beringia, edited by D. M. Hopkins, J. V. Matthews, C. E. Schweger, and S. B. Young, pp. 3–28, Academic Press., 1982.

Hopkins, D. M., McCulloch, D. S. and Jandra, R. J.: Pleistocene stratigraphy and structure of Baldwin Peninsula, Kotzebue Sound, Geol. Soc. Am. Spec. Pap. 68, 150–151, 1961.

Hugelius, G., Strauss, J., Zubrzycki, S., Harden, J. W., Schuur, E. A. G., Ping, C.-L., Schirrmeister, L., Grosse, G., Michaelson, G. J., Koven, C. D., O'Donnell, J. A., Elberling, B., Mishra, U., Camill, P., Yu, Z., Palmtag, J. and Kuhry, P.: Estimated stocks of circumpolar permafrost carbon with quantified uncertainty ranges and identified data gaps, Biogeosciences, 11(23), 6573–6593, doi:10.5194/bg-11-6573-2014, 2014.

Huston, M. M., Brigham-Grette, J. and Hopkins, D. M.: Paleogeographic significance of middle Pleistocene glaciomarine deposits on Baldwin Peninsula, northwest Alaska, Ann. Glaciol., 14(1), 111–114, 1990.

Jones, B. M. and Arp, C. D.: Observing a Catastrophic Thermokarst Lake Drainage in Northern Alaska, Permafr. Periglac. Process., 26(2), 119–128, doi:10.1002/ppp.1842, 2015.

Jones, M. C., Grosse, G., Jones, B. M. and Walter Anthony, K.: Peat accumulation in drained thermokarst lake basins in continuous, ice-rich permafrost, northern Seward Peninsula, Alaska, J. Geophys. Res. Biogeosciences, 117(G2), n/a–n/a, doi:10.1029/2011JG001766, 2012.

Jongejans, L. L., Strauss, J., Lenz, J., Peterse, F., Mangelsdorf, K., Fuchs, M. and Grosse, G.: Sedimentological, biogeochemical and geochronological data of yedoma and thermokarst deposits in West-Alaska, [online] Available from: https://doi.pangaea.de/10.1594/PANGAEA.892310, 2018.

Jorgenson, M., Yoshikawa, K., Kanevskiy, M., Shur, Y., Romanovsky, V., Marchenko, S., Grosse, G., Brown, J. and Jones, B.: Permafrost characteristics of Alaska, in Proceedings of the Ninth International Conference on Permafrost, vol. 29, pp. 121–122, University of Alaska: Fairbanks., 2008.

Kanevskiy, M., Shur, Y., Fortier, D., Jorgenson, M. T. and Stephani, E.: Cryostratigraphy of late Pleistocene syngenetic permafrost (yedoma) in northern Alaska, Itkillik River exposure, Quat. Res., 75(3), 584–596, doi:https://doi.org/10.1016/j.yqres.2010.12.003, 2011.

Kanevskiy, M., Shur, Y., Strauss, J., Jorgenson, T., Fortier, D., Stephani, E. and Vasiliev, A.: Patterns and rates of riverbank erosion involving ice-rich permafrost (yedoma) in northern Alaska, Geomorphology, 253, 370–384, doi:https://doi.org/10.1016/j.geomorph.2015.10.023, 2016.

Killops, S. D. and Killops, V. J.: Introduction to Organic Geochemistry, [online] Available from: http://nbn-resolving.de/urn:nbn:de:101:1-201410286047, 2013.

Knoblauch, C., Beer, C., Sosnin, A., Wagner, D. and Pfeiffer, E.-M.: Predicting long-term carbon mineralization and trace gas production from thawing permafrost of Northeast Siberia, Glob. Change Biol., 19(4), 1160–1172, doi:10.1111/gcb.12116, 2013.

Koven, C. D., Schuur, E. A. G., Schädel, C., Bohn, T. J., Burke, E. J., Chen, G., Chen, X., Ciais, P., Grosse, G., Harden, J. W., Hayes, D. J., Hugelius, G., Jafarov, E. E., Krinner, G., Kuhry, P., Lawrence, D. M., MacDougall, A. H., Marchenko, S. S., McGuire, A. D., Natali, S. M., Nicolsky, D. J., Olefeldt, D., Peng, S., Romanovsky, V. E., Schaefer, K. M., Strauss, J., Treat, C. C. and Turetsky, M.: A simplified, data-constrained approach to estimate the permafrost carbon–climate feedback, Philos. Trans. R. Soc. Math. Phys. Eng. Sci., 373(2054), doi:10.1098/rsta.2014.0423, 2015.

Lapointe, L. E., Talbot, J., Fortier, D., Fréchette, B., Strauss, J., Kanevskiy, M. and Shur, Y.: Middle to late Wisconsinan climate and ecological changes in northern Alaska: Evidences from the Itkillik River Yedoma, Palaeogeogr. Palaeoclimatol. Palaeoecol., 485, 906–916, doi:https://doi.org/10.1016/j.palaeo.2017.08.006, 2017.

Lawrence, D. M. and Slater, A. G.: A projection of severe near-surface permafrost degradation during the 21st century, Geophys. Res. Lett., 32(24), 1–5, doi:10.1029/2005GL025080, 2005.

Lee, H., Schuur, E. A. G., Inglett, K. S., Lavoie, M. and Chanton, J. P.: The rate of permafrost carbon release under aerobic and anaerobic conditions and its potential effects on climate, Glob. Change Biol., 18(2), 515–527, doi:10.1111/j.1365-2486.2011.02519.x, 2012.

Lenz, J., Wetterich, S., Jones, B. M., Meyer, H., Bobrov, A. and Grosse, G.: Evidence of multiple thermokarst lake generations from an 11 800-year-old permafrost core on the northern Seward Peninsula, Alaska, Boreas, 45(4), 584–603, doi:10.1111/bor.12186, 2016a.

Lenz, J., Jones, B. M., Wetterich, S., Tjallingii, R., Fritz, M., Arp, C. D., Rudaya, N. and Grosse, G.: Impacts of shore expansion and catchment characteristics on lacustrine thermokarst records in permafrost lowlands, Alaska Arctic Coastal Plain, arktos, 2(1), 25, doi:10.1007/s41063-016-0025-0, 2016b.

Lenz, J., Grosse, G., Jones, B. M., Walter Anthony, K. M., Bobrov, A., Wulf, S. and Wetterich, S.: Mid-Wisconsin to Holocene Permafrost and Landscape Dynamics based on a Drained Lake Basin Core from the Northern Seward Peninsula, Northwest Alaska, Permafr. Periglac. Process., 27(1), 56–75, doi:10.1002/ppp.1848, 2016c.

Lenz, J., Jones, B. M., Fuchs, M. and Grosse, G.: C/N and d13C data from short sediment cores from 9 lakes in Western Alaska, [online] Available from: https://doi.pangaea.de/10.1594/PANGAEA.887848, 2018.

Lide, D. R.: CRC handbook of chemistry and physics : a ready-reference book of chemical and physical data, CRC Press, Boca Raton., 1999.

Lindgren, P., Grosse, G. and Romanovsky, V.: Landsat-Based Lake Distribution and Changes in Western Alaska Permafrost Regions Between 1972 and 2014, in XI. International Conference on Permafrost, Potsdam, Germany. [online] Available from: http://epic.awi.de/42543/, 2016.

Marzi, R., Torkelson, B. E. and Olson, R. K.: A revised carbon preference index, Org. Geochem., 20(8), 1303–1306, doi:https://doi.org/10.1016/0146-6380(93)90016-5, 1993.

Meyers, P. A.: Preservation of elemental and isotopic source identification of sedimentary organic matter, Chem. Geol., 114(3), 289–302, doi:https://doi.org/10.1016/0009-2541(94)90059-0, 1994.

Meyers, P. A.: Organic geochemical proxies of paleoceanographic, paleolimnologic, and paleoclimatic processes, Org. Geochem., 27(5), 213–250, doi:https://doi.org/10.1016/S0146-6380(97)00049-1, 1997.

Morgenstern, A., Grosse, G., Günther, F., Fedorova, I. and Schirrmeister, L.: Spatial analyses of thermokarst lakes and basins in Yedoma landscapes of the Lena Delta, Cryosphere Discuss., 5, 1495–1545, doi:10.5194/tcd-5-1495-2011, 2011.

Mueller, C. W., Rethemeyer, J., Kao-Kniffin, J., Löppmann, S., Hinkel, K. M. and G Bockheim, J.: Large amounts of labile organic carbon in permafrost soils of northern Alaska, Glob. Change Biol., 21(7), 2804–2817, 2015.

Overland, J., Hanna, E., Hanssen-Bauer, I., Kim, S.-J., Walsh, J., Wang, M., Bhatt, U. S. and Thoman, R. L.: Surface Air Temperature, in http://www.arctic.noaa.gov/Report-Card/Report-Card-2017. [online] Available from: http://arctic.noaa.gov/Report-Card, 2017.

Peters, K. E., Walters, C. C. and Moldowan, J. M.: The biomarker guide, 1, Biomarkers and isotopes in the environment and human history, 2005.

Poynter, J. and Eglinton, G.: 14. Molecular composition of three sediments from hole 717c: The Bengal fan, in Proceedings of the Ocean Drilling Program: Scientific results, vol. 116, pp. 155–161, College Station, TX., 1990.

Pushkar, V. S., Roof, S. R., Cherepanova, M. V., Hopkins, D. M. and Brigham-Grette, J.: Paleogeographic and paleoclimatic significance of diatoms from middle Pleistocene marine and glaciomarine deposits on Baldwin Peninsula, northwestern Alaska, Palaeogeogr. Palaeoclimatol. Palaeoecol., 152(1), 67–85, doi:https://doi.org/10.1016/S0031-0182(99)00040-1, 1999.

Radke, M., Willsch, H. and Welte, D. H.: Preparative hydrocarbon group type determination by automated medium pressure liquid chromatography, Anal. Chem., 52(3), 406–411, 1980.

Rowell, D. L.: Soil Science: methods & applications., Longman Scientific & Technical, University of Michigan., 1994.

Sánchez-García, L., Vonk, J. E., Charkin, A. N., Kosmach, D., Dudarev, O. V., Semiletov, I. P. and Gustafsson, Ö.: Characterisation of Three Regimes of Collapsing Arctic Ice Complex Deposits on the SE Laptev Sea Coast using Biomarkers and Dual Carbon Isotopes, Permafr. Periglac. Process., 25(3), 172–183, doi:10.1002/ppp.1815, 2014.

Schädel, C., Schuur, E. A. G., Bracho, R., Elberling, B., Knoblauch, C., Lee, H., Luo, Y., Shaver, G. R. and Turetsky, M. R.: Circumpolar assessment of permafrost C quality and its vulnerability over time using long-term incubation data, Glob. Change Biol., 20(2), 641–652, doi:10.1111/gcb.12417, 2014a.

Schädel, C., Schuur, E. A. G., Bracho, R., Elberling, B., Knoblauch, C., Lee, H., Luo, Y., Shaver, G. R. and Turetsky, M. R.: Circumpolar assessment of permafrost C quality and its vulnerability over time using long-term incubation data, Glob. Change Biol., 20(2), 641–652, doi:10.1111/gcb.12417, 2014b.

Schirrmeister, L., Siegert, C., Kunitzky, V. V., Grootes, P. M. and Erlenkeuser, H.: Late Quaternary ice-rich permafrost sequences as a paleoenvironmental archive for the Laptev Sea Region in northern Siberia, Int. J. Earth Sci., 91(1), 154–167, 2002a.

Schirrmeister, L., Siegert, C., Kuznetsova, T., Kuzmina, S., Andreev, A., Kienast, F., Meyer, H. and Bobrov, A.: Paleoenvironmental and paleoclimatic records from permafrost deposits in the Arctic region of Northern Siberia, Quat. Int., 89(1), 97–118, doi:https://doi.org/10.1016/S1040-6182(01)00083-0, 2002b.

Schirrmeister, L., Grosse, G., Schwamborn, G., Andreev, A., Meyer, H., Kunitsky, V. V., Kuznetsova, T., Dorozhkina, M. V., Pavlova, E. Y., Bobrov, A. and Oezen, D.: Late Quaternary history of the accumulation plain north of the Chekanovsky Ridge (Lena Delta, Russia) - a multidisciplinary approach, Polar Geogr., 27(4), 277–319, 2003.

Schirrmeister, L., Grosse, G., Kunitsky, V., Magens, D., Meyer, H., Dereviagin, A., Kuznetsova, T., Andreev, A., Babiy, O., Kienast, F., Grigoriev, M., Overduin, P. P. and Preusser, F.: Periglacial landscape evolution and environmental changes of Arctic lowland areas for the last 60 000 years (western Laptev Sea coast, Cape Mamontov Klyk), Polar Res., 27(2), 249–272, doi:10.1111/j.1751-8369.2008.00067.x, 2008a.

Schirrmeister, L., Kunitsky, V. V., Grosse, G., Kuznetsova, T. V., Derevyagin, A. Y., Wetterich, S. and Siegert, C.: The Yedoma Suite of the Northeastern Siberian Shelf Region characteristics and concept of formation, in Proceedings of the Ninth International Conference on Permafrost, Fairbanks, Alaska., 2008b.

Schirrmeister, L., Grosse, G., Wetterich, S., Overduin, P. P., Strauss, J., Schuur, E. A. G. and Hubberten, H.-W.: Fossil organic matter characteristics in permafrost deposits of the northeast Siberian Arctic, J. Geophys. Res. Biogeosciences, 116(G2), 1–16, doi:10.1029/2011JG001647, 2011.

Schirrmeister, L., Froese, D., Tumskoy, V., Grosse, G. and Wetterich, S.: Yedoma: Late Pleistocene ice-rich syngenetic permafrost of Beringia, edited by S. A. Elias, C. J. Mock, and J. Murton, Elsevier, Amsterdam., 2013.

Schulte, S., Mangelsdorf, K. and Rullkötter, J.: Organic matter preservation on the Pakistan continental margin as revealed by biomarker geochemistry, Org. Geochem., 31(10), 1005–1022, doi:https://doi.org/10.1016/S0146-6380(00)00108-X, 2000.

Schuur, E. A., Vogel, J. G., Crummer, K. G., Lee, H., Sickman, J. O. and Osterkamp, T.: The effect of permafrost thaw on old carbon release and net carbon exchange from tundra, Nature, 459(7246), 556, 2009.

Schuur, E. A. G., McGuire, A. D., Schädel, C., Grosse, G., Harden, J. W., Hayes, D. J., Hugelius, G., Koven, C. D., Kuhry, P., Lawrence, D. M., Natali, S. M., Olefeldt, D., Romanovsky, V. E., Schaefer, K., Turetsky, M. R., Treat, C. C. and Vonk, J. E.: Climate change and the permafrost carbon feedback, Nature, 520, 171, 2015.

Sher, A. V.: Yedoma as a store of paleoenvironmental records in Beringia, in Beringia Palaeoenvironmental Workshop, edited by S. Elias and J. Bringham-Grette, pp. 92–94, ON, Canada., 1997.

Shmelev, D., Veremeeva, A., Kraev, G., Kholodov, A., Spencer, R. G. M., Walker, W. S. and Rivkina, E.: Estimation and Sensitivity of Carbon Storage in Permafrost of North-Eastern Yakutia, Permafr. Periglac. Process., 28(2), 379–390, doi:10.1002/ppp.1933, 2017.

Shur, Y., Kanevskiy, M., Jorgenson, T., Dillon, M., Stephani, E., Bray, M. and Fortier, D.: Permafrost degradation and thaw settlement under lakes in yedoma environment, in Proceedings of the Tenth International Conference on Permafrost, vol. 1, pp. 25–29, Salekhard, Russia., 2012.

Siewert, M. B., Hugelius, G., Heim, B. and Faucherre, S.: Landscape controls and vertical variability of soil organic carbon storage in permafrost-affected soils of the Lena River Delta, CATENA, 147, 725–741, doi:https://doi.org/10.1016/j.catena.2016.07.048, 2016.

Stapel, J. G., Schirrmeister, L., Overduin, P. P., Wetterich, S., Strauss, J., Horsfield, B. and Mangelsdorf, K.: Microbial lipid signatures and substrate potential of organic matter in permafrost deposits: Implications for future greenhouse gas production, J. Geophys. Res. Biogeosciences, 121(10), 2652–2666, doi:10.1002/2016JG003483, 2016.

Strauss, J., Schirrmeister, L., Wetterich, S., Borchers, A. and Davydov, S. P.: Grain-size properties and organic-carbon stock of Yedoma Ice Complex permafrost from the Kolyma lowland, northeastern Siberia, Glob. Biogeochem. Cycles, 26(3), doi:10.1029/2011GB004104, 2012.

Strauss, J., Schirrmeister, L., Grosse, G., Wetterich, S., Ulrich, M., Herzschuh, U. and Hubberten, H.-W.: The deep permafrost carbon pool of the Yedoma region in Siberia and Alaska, Geophys. Res. Lett., 40(23), 6165–6170, doi:10.1002/2013GL058088, 2013.

Strauss, J., Schirrmeister, L., Mangelsdorf, K., Eichhorn, L., Wetterich, S. and Herzschuh, U.: Organic-matter quality of deep permafrost carbon - a study from Arctic Siberia, Biogeosciences, 12, 2227–2245, doi:10.5194/bg-12-2227-2015, 2015.

Strauss, J., Schirrmeister, L., Grosse, G., Fortier, D., Hugelius, G., Knoblauch, C., Romanovsky, V., Schädel, C., Deimling, T. S. von, Schuur, E. A. G., Shmelev, D., Ulrich, M. and Veremeeva, A.: Deep Yedoma permafrost: A synthesis of depositional characteristics and carbon vulnerability, Earth-Sci. Rev., 172, 75–86, doi:https://doi.org/10.1016/j.earscirev.2017.07.007, 2017.

Stuiver, M., Reimer, P. J. and Reimer, R. W.: CALIB 14C Calibration Program, [online] Available from: http://calib.org/calib/ (Accessed 13 December 2017), 2017.

Ulrich, M., Grosse, G., Strauss, J. and Schirrmeister, L.: Quantifying Wedge-Ice Volumes in Yedoma and Thermokarst Basin Deposits, Permafr. Periglac. Process., 25(3), 151–161, doi:10.1002/ppp.1810, 2014.

US Climate Data: Climate Kotzebue - Alaska, [online] Available from: https://www.usclimatedata.com/climate/kotzebue/alaska/united-states/usak0135/2017/1, 2017.

Vasil'chuk, Y. K. and Vasil'chuk, A. C.: Validity of radiocarbon ages of Siberian yedoma, GeoResJ, 13(Supplement C), 83–95, doi:https://doi.org/10.1016/j.grj.2017.02.004, 2017.

Vonk, J. E., Van Dongen, B. E. and Gustafsson, Ö.: Selective preservation of old organic carbon fluvially released from sub-Arctic soils, Geophys. Res. Lett., 37(11), 2010.

Vonk, J. E., Mann, P. J., Davydov, S., Davydova, A., Spencer, R. G. M., Schade, J., Sobczak, W. V., Zimov, N., Zimov, S., Bulygina, E., Eglinton, T. I. and Holmes, R. M.: High biolability of ancient permafrost carbon upon thaw, Geophys. Res. Lett., 40(11), 2689–2693, doi:10.1002/grl.50348, 2013.

Walter Anthony, K. M., Zimov, S. A., Grosse, G., Jones, M. C., Anthony, P. M., III, F. S. C., Finlay, J. C., Mack, M. C., Davydov, S., Frenzel, P. and Frolking, S.: A shift of thermokarst lakes from carbon sources to sinks during the Holocene epoch, Nature, 511, 452, 2014.

Webb, E. E., Heard, K., Natali, S. M., Bunn, A. G., Alexander, H. D., Berner, L. T., Kholodov, A., Loranty, M. M., Schade, J. D., Spektor, V. and Zimov, N.: Variability in above- and belowground carbon stocks\hack\newline in a Siberian larch watershed, Biogeosciences, 14(18), 4279–4294, doi:10.5194/bg-14-4279-2017, 2017.

Weiss, N., Blok, D., Elberling, B., Hugelius, G., Jørgensen, C. J., Siewert, M. B. and Kuhry, P.: Thermokarst dynamics and soil organic matter characteristics controlling initial carbon release from permafrost soils in the Siberian Yedoma region, Sediment. Geol., 340, 38–48, doi:10.1016/j.sedgeo.2015.12.004, 2016a.

Weiss, N., Blok, D., Elberling, B., Hugelius, G., Jørgensen, C. J., Siewert, M. B. and Kuhry, P.: Thermokarst dynamics and soil organic matter characteristics controlling initial carbon release from permafrost soils in the Siberian Yedoma region, Sediment. Geol., 340, 38–48, doi:https://doi.org/10.1016/j.sedgeo.2015.12.004, 2016b.

Zimov, S. A., Davydov, S. P., Zimova, G. M., Davydova, A. I., Schuur, E. A. G., Dutta, K. and Chapin, F. S.: Permafrost carbon: Stock and decomposability of a globally significant carbon pool, Geophys. Res. Lett., 33(20), doi:10.1029/2006GL027484, 2006.

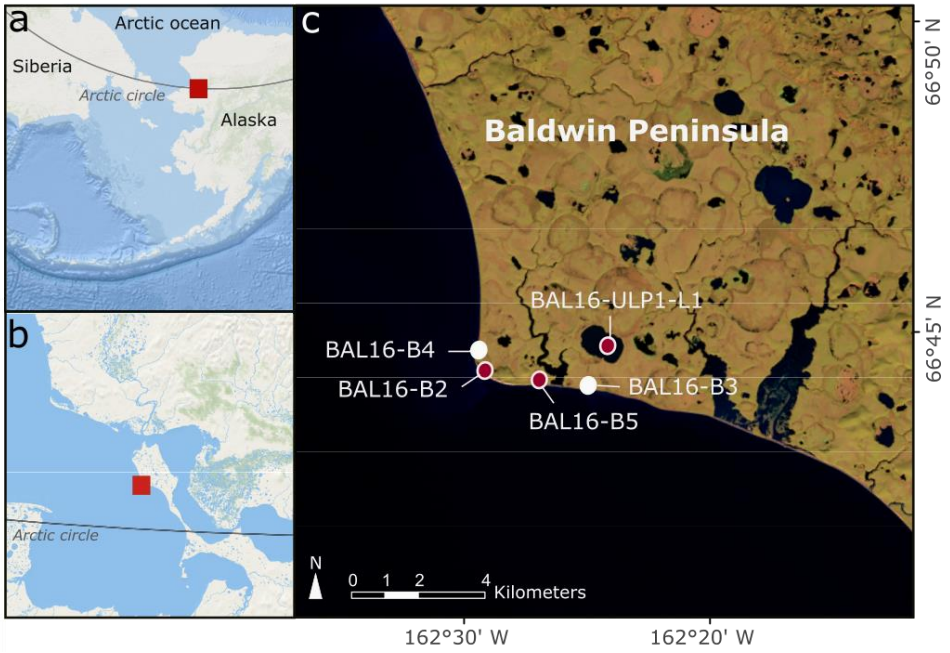

Figure 1: (a) Overview map of Siberia and Alaska with indicated study region (red square). (b) Close-up of Kotzebue Sound with indicated study region (red square). (c) Study sites on Baldwin Peninsula presented in this study (purple filled dots) and additional sites used in the organic carbon pool calculations (white dots); false color image with short-wave infrared, near-infrared and deep blue bands (7-5-1). Source for background map in (a) and (b): World Ocean Base (ESRI); satellite image map (c): Landsat 8 image from 13 Oct. 2016, USGS/NASA.

Table 1: Overview of study sites of yedoma exposure, drained thermokarst lake basin (DTLB) exposure and thermokarst lake sediments. BAL: Baldwin Peninsula, 16: expedition in 2016, B: bluff sampling, UPL: upland sampling, L: lake sampling.

Study site ID	Landscape unit	Coordinates	Samples, n
BAL16-B2	Yedoma exposure	66.73262°N, 62.49450°W	18
BAL16-B4	DTLB exposure	66.73644°N, 62.50208°W	31
BAL16-UPL1-L1	Thermokarst lake sediments	66.74220°N, 62.41310°W	9

Table 2: Radiocarbon dates of BAL16-B2 (yedoma), BAL16-B4 (drained thermokarst lake basin) and BAL16-UPL1-L1 (thermokarst lake). Calibrations were performed using CALIB 7.1 software and the IntCal13 calibration curve (Stuiver et al., 2017). ±: standard deviation, **Poz: Poznan Radiocarbon Laboratory, Poland, pMC: percent modern carbon.**

Field Code Changed

Sample ID	Ext. ID	Depth [cm]	^{14}C ages [a BP]	±	Calibrated ages 2σ (95.4 %) [a BP]	±	Rounded ^{14}C ages [cal a BP]	±
BAL16-B2-20	Poz-89527	620	> 48,000					
BAL16-B2-26	Poz-89700	945	8,890	50	10,037.5	307	10,000	310
BAL16-B2-31	Poz-89702	1117	40,810	1800	44,747	6250	44,700	6250
BAL16-B2-39	Poz-89703	1399	> 50,000					
BAL16-B2-1	Poz-89526	1500	> 50,000					
BAL16-B2-5	Poz-89523	1600	16,200	90	19,551.5	575	19,600	580
BAL16-B4-2a	Poz-89704	22	105.7	0.33 pMC	239	30	240	30
BAL16-B4-4a	Poz-89705	132	1,700	30	1,590.5	93	1,590	90
BAL16-B4-6a	Poz-89706	166	2,125	30	2,079.5	155	2,080	160
BAL16-B4-14a	Poz-89707	340	42,800	1,600	46,361.5	5935	46,400	6000
BAL16-B4-18a	Poz-89708	434	> 50,000					
BAL16-B4-24a	Poz-89709	583	> 50,000					
BAL16-B4-31a	Poz-89710	788	> 50,000					
BAL16-UPL1-L1-A	Poz-89349	19-20	425	30	482	86	480	90
BAL16-UPL1-L1-B	Poz-89351	26.5-27.5	1,940	30	2,014.5	129	2,015	130

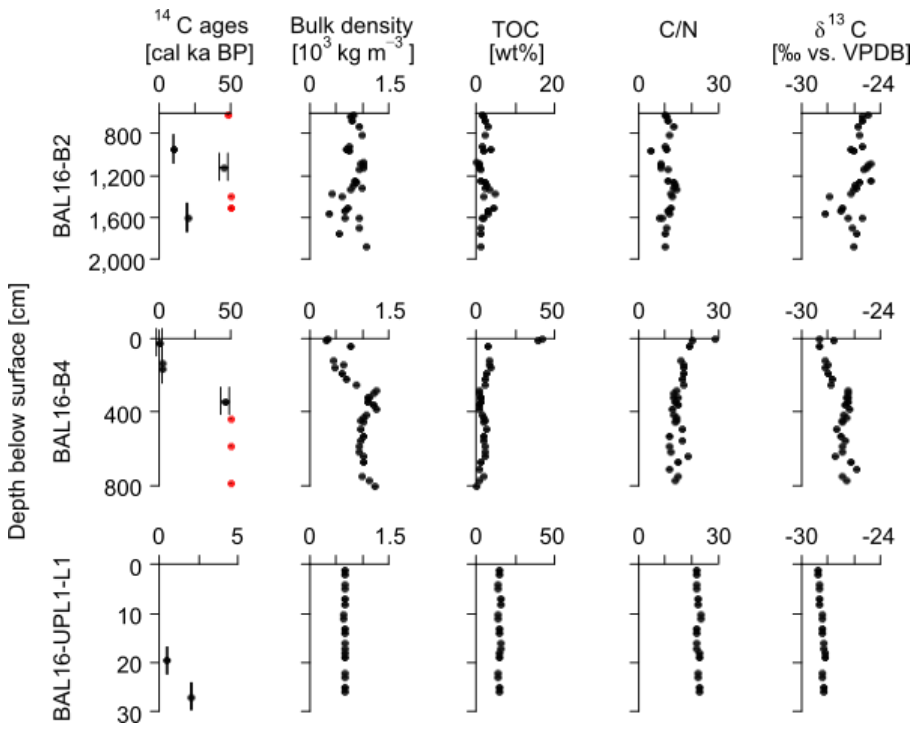

Figure 2: Summary of cryostratigraphical and biogeochemical parameters of BAL16-B2 (yedoma), BAL16-B4 (drained thermokarst lake basin) and BAL16-UPL1-L1 (thermokarst lake): calibrated radiocarbon ages (^{14}C; infinite ages in red), bulk density, total organic carbon (TOC), total organic carbon-total nitrogen ratio (C/N), stable carbon isotopes (δ^{13}C). Note: different x-axes for ^{14}C and TOC.

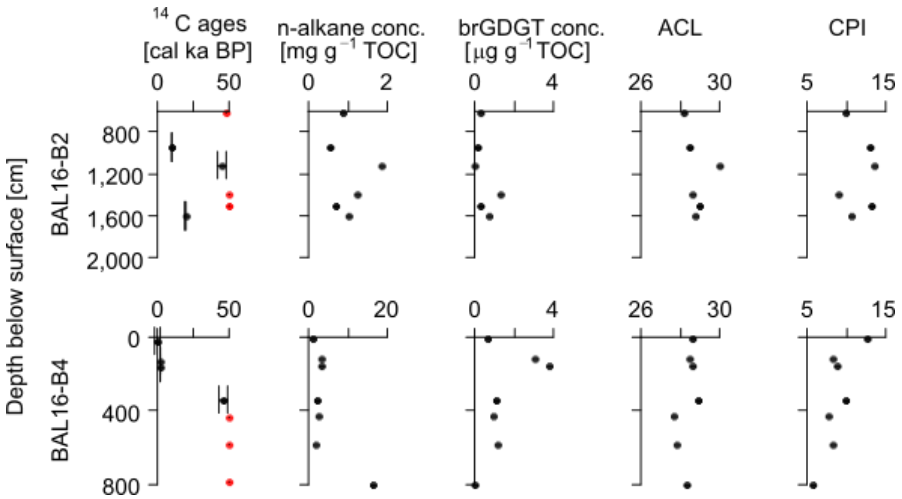

Figure 3: Summary of biomarker parameters of BAL16-B2 (yedoma) and BAL16-B4 (drained thermokarst lake basin): calibrated radiocarbon ages (^{14}C; infinite ages in red), *n*-alkane concentration, brGDGT concentration, average chain length (ACL) and carbon preference index (CPI). ACL and CPI were calculated from *n*-alkane range C_{23-33}. Note: radiocarbon ages are the same as in Figure 2; different x-axes for *n*-alkane concentration.

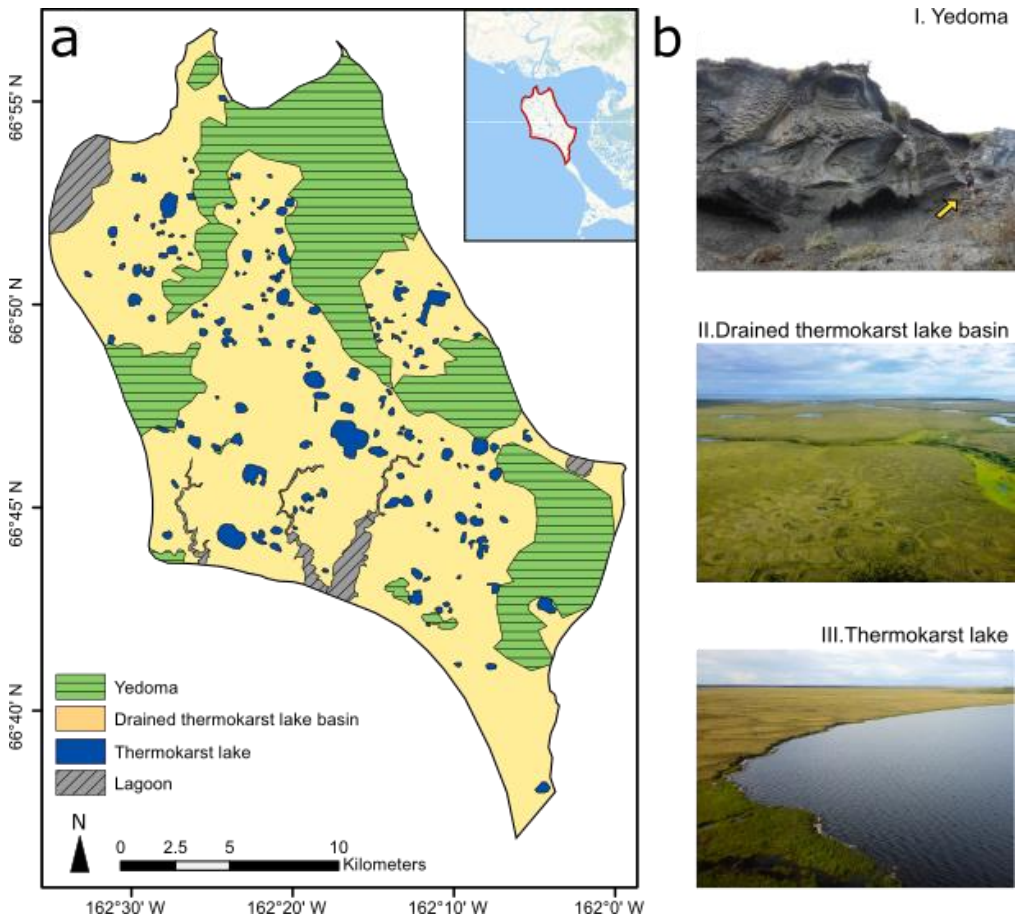

Figure 4: a) Land cover classification map of Baldwin Peninsula (see overview map in upper-right corner) with yedoma (green), drained thermokarst lake basins (yellow), thermokarst lakes (blue) and lagoons (grey). B) Exemplary photos: I. Yedoma (note person on the right indicated by yellow arrow for scale), II. Drained thermokarst lake basin and III. Thermokarst lake. Source for overview map in (a): World Ocean Base (ESRI).

Table 3: Input (left) and output parameters (right) for organic carbon pool calculations for yedoma, drained thermokarst lake basin and thermokarst lake deposits: deposit thickness, landscape coverage, wedge-ice volume (WIV), average weighted bulk density * total organic carbon (BD*TOC). WIV data from Ulrich et al. (2014).

Field Code Changed

Landscape unit	Thickness	Coverage	WIV	Volumetric OC pool Incl. WIV	Total OC pool Incl. WIV	Volumetric OC pool excl. WIV	Total OC pool excl. WIV
	[m]	[m^2]	[vol %]	[kg m^{-3}]	[Mt]	[kg m^{-3}]	[Mt]
Yedoma	15	136,620,000	48	8.0 ± 0.8	16.3 ± 1.7	15.3 ± 1.6	31.4 ± 3.3
DTLB	5	296,440,000	7	34.7 ± 2.9	51.5 ± 4.3	37.4 ± 3.1	55.4 ± 4.6
Thermokarst lake	2	21,180,000	0			92.9 ± 0.8	3.9 ± 0.0

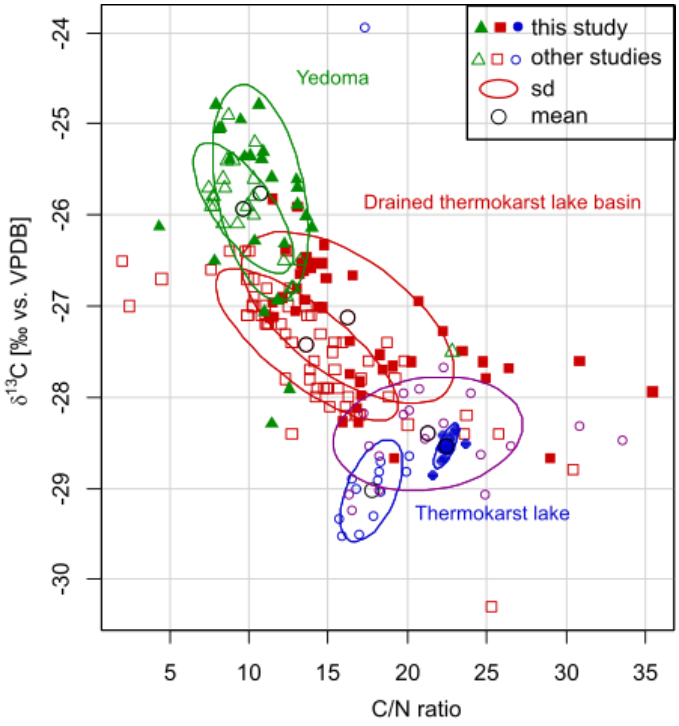

Figure 5: Scatterplot of total organic carbon-total nitrogen (C/N) ratio and stable carbon isotopes ($\delta^{13}C$) of yedoma deposits (green triangles), drained thermokarst lake basin (DTLB) deposits (red squares) and thermokarst lake sediments (blue and purple dots) in Alaska. Mean value and standard deviation (sd) indicated. Data from this study (filled symbols): Baldwin Peninsula; data from other studies (hollow symbols): Itkillik River (Lapointe et al., 2017; Strauss et al., 2012), Northern Seward Peninsula (Lenz et al., 2016a) and lakes from Kobuk River Delta (blue) and Central Seward Peninsula (purple) (Lenz et al., 2018).

Field Code Changed

Field Code Changed

Field Code Changed

Supplementary Materials for "Organic matter characteristics in yedoma and thermokarst deposits on Baldwin Peninsula, West-Alaska"

Loeka L. Jongejans[1], Jens Strauss[1], Josefine Lenz[1,2], Francien Peterse[3], Kai Mangelsdorf[4], Matthias Fuchs[1,5] and Guido Grosse[1,5]

[1]Alfred Wegener Institute Helmholtz Centre for Polar and Marine Research, Periglacial Research Section, Potsdam, Germany
[2] University of Alaska Fairbanks, Institute of Northern Engineering, Fairbanks, USA
[3] Utrecht University, Department of Earth Sciences, Utrecht, Netherlands
[4] Helmholtz Centre Potsdam - German Research Centre for Geosciences
[5] University of Potsdam, Institute of Earth and Environmental Sciences, Potsdam, Germany

Correspondence to: Loeka L. Jongejans (loeka.jongejans@awi.de)

Contents of Supplementary Materials

1 Supporting methodology descriptions

1.1 Grain size analysis

The analysis of grain size is important in identifying the origin of sedimentary deposits: grain size distributions of the sedimentary sediments can give insights into the medium of transportation, as well as the depositional mechanism. Grain size was analyzed for yedoma exposure BAL16-B2 and drained thermokarst lake basin exposure BAL16-B4. In order to only measure the clastic material, organic matter was removed from the samples by treating the samples with hydrogen peroxide (H_2O_2). For this, about 10 ml of sample material was weighed into 400 ml beakers to which 100 ml of 3% H_2O_2 and 4 drops of ammonia were added. The beakers were then placed on a shaker at 60°C for 2-3 weeks. Five times a week, the beakers were cleaned and 10 ml of H_2O_2 was added (once the reaction was less strong 20 ml was added). The pH was kept between 6 and 8 by adding ammonia or acetic acid to allow an optimal reaction. After the complete removal of the organic material, the samples were washed with about one liter of purified water to remove the H_2O_2. The samples were then centrifuged (Cryofuge 8500i for 10 minutes at 5050 RPM, 20°C; Multifuge 3-S Heraeus 2-3 times for 15 minutes at 4000 RPM) and freeze-dried. The samples were manually homogenized and about 1 gram was weighed into 250 ml plastic bottles and a spoon spatula of dispersing agent (tetrasodium pyrophosphate, $Na_4P_2O_7$) was added. The bottles were filled with an ammonia solution (10 ml NH_4OH in 100 liter of water) and placed in an overhead shaker overnight. As a last step before measuring, the samples were split into 8 homogeneous samples to enable measurement of samples with sediment concentrations between 5-15%. The material was hereby also sieved for >1 mm to avoid damage to the laser. Inorganic particles >1mm were weighed and if the residue was significant compared to the sample, it was included in the distribution afterwards. The grain size was analyzed with the Malvern Mastersizer 3000 laser. The device cleans automatically and measures background scatter. After a sample is inserted into the dispersion unit, it is channeled through the device to the measurement cell where it is exposed to a red laser and blue led (633 nm and 470 nm), of which the scatter is measured by the detectors. The average is calculated of three measurements per split sample (standard deviation <10%). Grain size statistics are calculated using the software GRADISTAT using the grain size scaling from Blott & Pey (2001).

1.2 Elemental analysis

Total carbon (TC), total nitrogen (TN) and total organic carbon (TOC) are measured based on the principle of combustion chromatography. TC and TN were determined using the Elementar Vario EL III. A subsample of each homogenized sample was weighed into small tin capsules in duplicate. A blank capsule was measured in the beginning for background detection and a calibration run was performed before and after every fifteen samples. The percentage of total carbon and nitrogen was calculated. The determination of TOC was done using the Elementar Vario Max C. Depending on the TC values, fifteen to hundred milligrams of the samples was weighed into crucibles and placed into the machine. TN, TC and TOC are expressed in weight percentage (wt%).

Stable carbon isotopes ($\delta^{13}C$) could be measured after the removal of carbonates. This was done by treating the samples with 20 ml hydrogen chloride for three hours at 97.7°C. Purified water was added and the samples were decanted and washed three times. When the chloride content was under 500 parts per million, the samples were filtered over a glass microfiber filter (Whatman Grade GF/B, nominal particle retention of 1.0 µm). Afterwards, the residue was dried in a drying cabinet at 50°C. Dry samples were ground manually and weighed into tin capsules. The required sample weight was calculated by dividing 20 by the TOC value. A ThermoFisher Scientific Delta-V-Advantage gas mass spectrometer equipped with a FLASH elemental analyzer EA 2000 and a CONFLO IV gas mixing system was used to determine the $\delta^{13}C$. In this system, the sample is combusted at 1020°C so that the OC is transferred to CO_2, after which the isotope ratio is determined relative to a laboratory standard of known isotopic composition. Capsules for control and calibration were run in between. The unit is per mille (‰) and the ratio is compared to the standard established from the Pee Dee Belemnite (VPDB: a limestone formation of which the ratio was set to 0).

1.3 Lipid biomarker analysis

From the GDGT concentration, the branched and isoprenoid tetraethers (BIT) index was calculated following Eq. (1).

$$BIT = \frac{Ia+IIa+IIIa}{Ia+IIa+IIIa+crenarchaeol} \quad (1)$$

The BIT index is the ratio between the mainly terrestrially produced brGDGTs and crenarchaeol (Figure S1), an isoprenoid GDGT which is most abundant in marine and lacustrine environments. Apart from the use of this proxy to distinguish between terrestrial and marine sources (Hopmans et al., 2004), the ratio is correlated to precipitation (Dirghangi et al., 2013). The methylation of branched tetraethers (MBT) index is the ratio between brGDGT-I and -II structures and was calculated according to Peterse et al. (2012) following Eq. (2).

$$MBT = \frac{Ia+Ib+Ic}{Ia+Ib+Ic+IIa+IIb+IIc+IIIa} \quad (2)$$

This ratio can be used in paleoreconstructions. Weijers et al. (2007) found that Arctic soils are generally dominated by brGDGTs with additional methyl branches and suggested that more methyl branches are formed in lower temperatures.

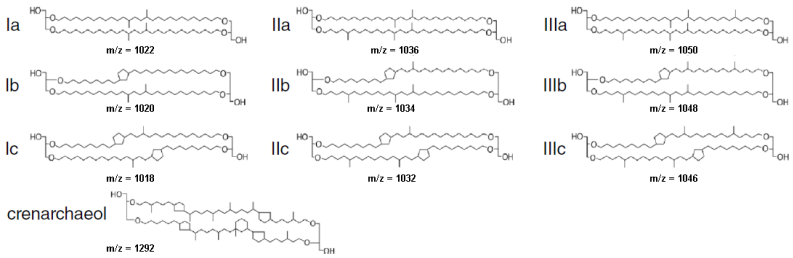

Figure S1: Molecular structures of brGDGTs and crenarchaeol with mass-to-charge ratio (m/z). The structures differ in mass by the presence of cyclopentane moieties (a, b, c) and the number of methyl branches (I, II, III). From Peterse et al. (2014).

2 Supporting figures and tables

2.1 Photographs field sites

Photographs of the field sites are shown for the yedoma exposure BAL16-B2 (Figure S2), drained thermokarst lake basin exposures BAL16-B3 (Figure S3) and BAL16-B4 (Figure S4) and the thermokarst lake core BAL16-UPL-L1 (Figure S5).

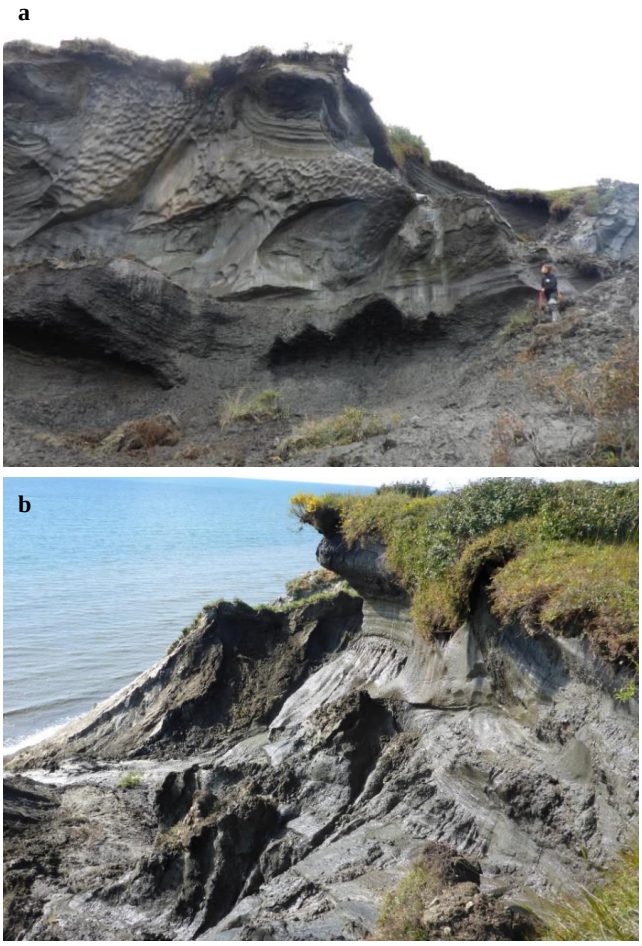

Figure S2: Yedoma exposure BAL16-B2 from the front (a) and side (b). Photos by J. Strauss, August 2016.

Figure S3: Drained thermokarst lake basin exposure BAL16-B3. Photo by J. Strauss, August 2016.

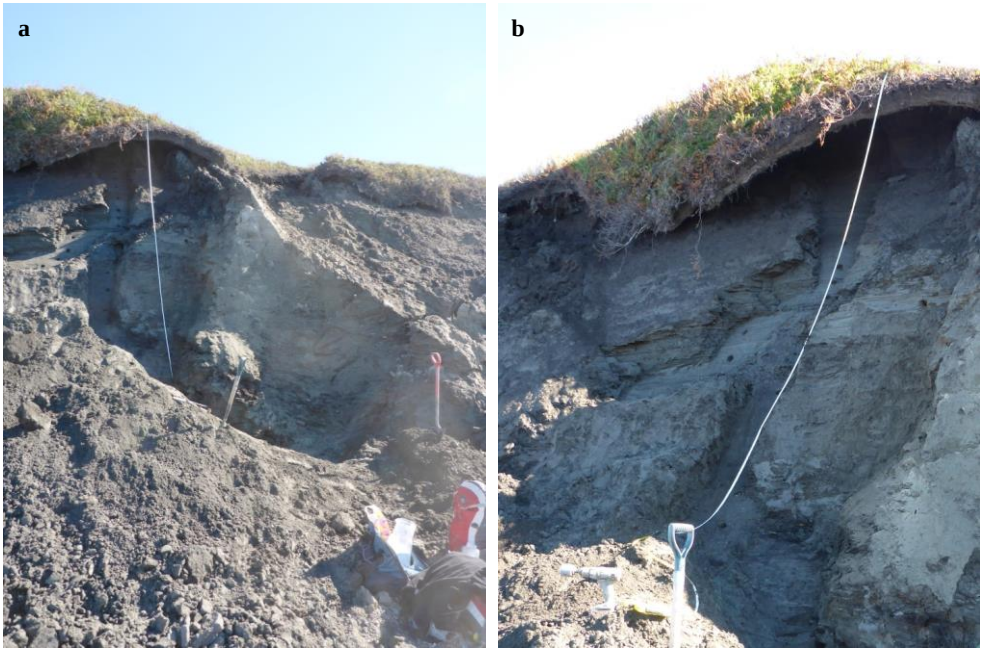

Figure S4: Drained thermokarst lake basin exposure BAL16-B4 from the front (a) and side (b). Photos by J. Strauss, August 2016.

Figure S5: Thermokarst lake core BAL16-UPL1-L1. Photo by J. Lenz, December 2016.

2.2 Total organic carbon

Figure S6 shows variations in total organic carbon of previously studied yedoma deposits in Siberia and Alaska.

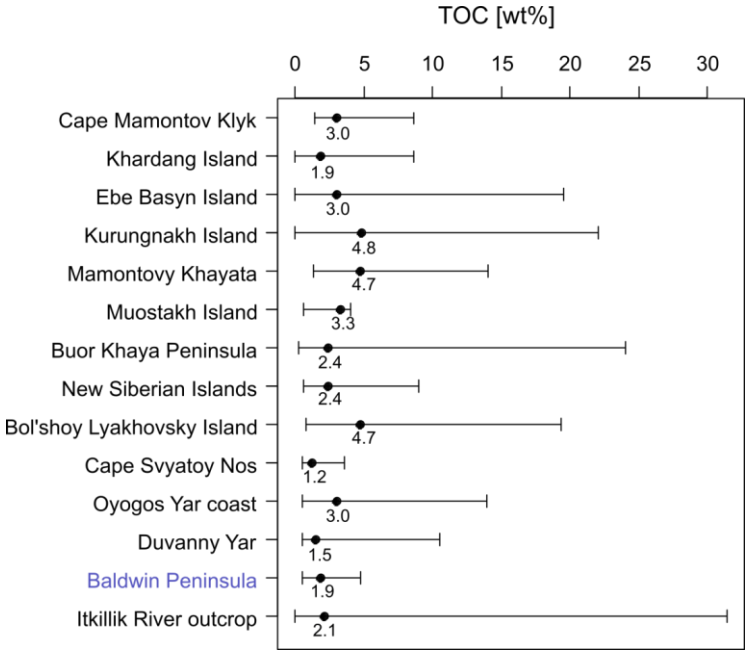

Figure S6: Total organic carbon (TOC) variations from different yedoma study sites in Siberia and Alaska. Sorted from westernmost (Cape Mamontov Klyk, western Laptev Sea) to easternmost (Itkillik River outcrop, Alaskan North Slope) study sites. Data from Schirrmeister et al. (2008a, 2008b, 2011), Strauss et al. (2012, 2013, 2015) and Baldwin Peninsula (this study; blue).

2.3 Additional profiles

Figure S7 shows the cryostratigraphical and biogeochemical parameters of the additional drained thermokarst lake basin exposures BAL16-B3 and BAL16-B5 that were used in the organic carbon calculations.

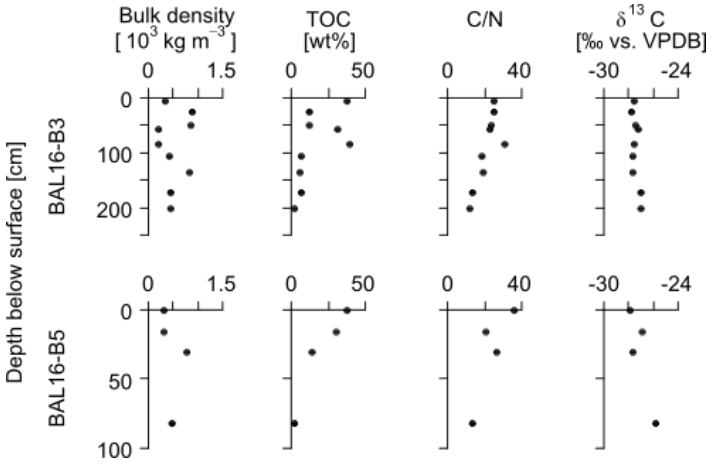

Figure S7: Summary of cryostratigraphical and biogeochemical parameters of BAL16-B3 and BAL16-B5 (drained thermokarst lake basin exposures): bulk density, total organic carbon (TOC), total organic carbon-total nitrogen ratio (C/N), stable carbon isotopes ($\delta^{13}C$).

2.4 *n*-Alkane concentration

The *n*-alkane concentrations per sample are shown in Figure S8. Also, the dominating *n*-C chain is indicated.

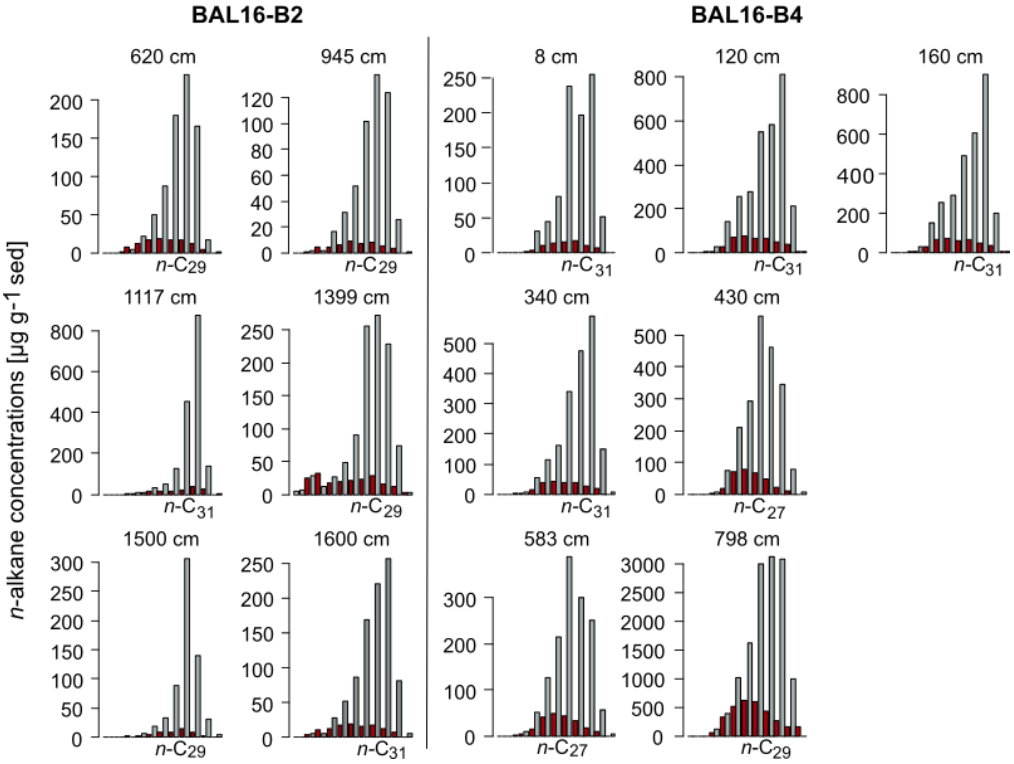

Figure S8: *n*-alkane concentrations of BAL16-B2 (yedoma) and BAL16-B4 (drained thermokarst lake basin) by depth. Odd chains (grey bars) and even chains (red bars), sample depth (above graph) and dominating *n*-chain indicated (below x-axis). Note: different y-axes.

2.5 Depositional environment

2.5.1 Grain size distribution

The grain size distributions of yedoma exposure BAL16-B2 and drained thermokarst lake basin exposure BAL16-B4 are shown in Figure S9 and Figure S10, respectively.

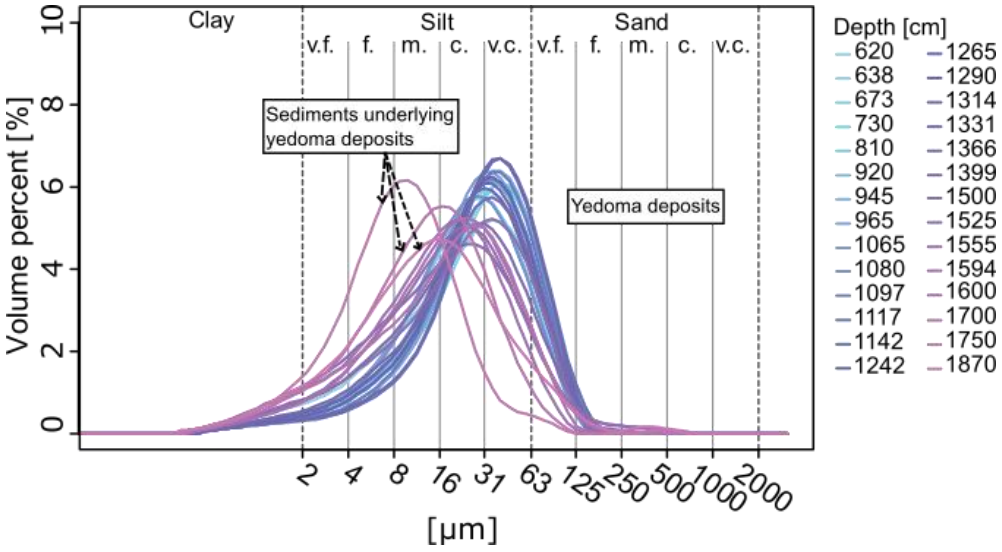

Figure S9: Grain size distribution of BAL16-B2 (yedoma). Samples sorted over depth (legend on the right). v.f.: very fine, f.: fine, m.: medium, c.: coarse, v.c.: very coarse. Sediments from the separate unit underlying the yedoma deposits indicated.

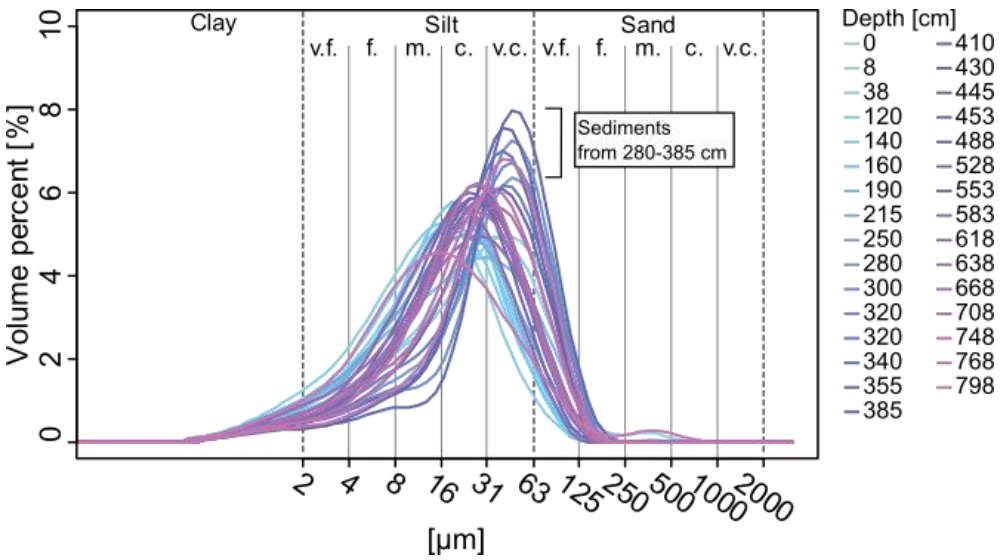

Figure S10: Grain size distribution of BAL16-B4 (drained thermokarst lake basin). Samples sorted over depth (legend on the right). v.f.: very fine, f.: fine, m.: medium, c.: coarse, v.c.: very coarse. Sediments from depth interval of 280-385 cm indicated.

2.5.2 Climatic indicators

Table S1 shows the brGDGT derived climatic indices BIT and MBT indices.

Table S1: brGDGT derived climatic indices for BAL16-B2 (yedoma) and BAL16-B4 (drained thermokarst lake basin): branched and isoprenoid tetraethers (BIT) index and methylation of branched tetraethers (MBT) index.

	Depth [cm]	BIT	MBT
Yedoma	620	0.90	0.19
	945	0.96	0.19
	1117	NA	NA
	1399	1.00	0.39
	1500	0.97	0.20
	1600	0.88	0.18
DTLB	8	1.00	0.25
	120	1.00	0.27
	160	1.00	0.30
	340	0.99	0.25
	430	1.00	0.22
	583	1.00	0.16
	798	NA	NA

2.6 Statistical tests

Using the Shapiro-Wilk test, we tested for normality of the data (Table S2). In this test, the null hypothesis states that the data are normally distributed. When the p-value exceeds 0.05, the null hypothesis cannot be rejected. Using the Kruskal-Wallis test, a non-parametric test, we tested for significant differences of the biogeochemical parameters (bulk density, total organic carbon, carbon-nitrogen ratio and stable carbon isotopes) between the three stratigraphic landscape units on Baldwin Peninsula (Table S2): yedoma, drained thermokarst lake basin and thermokarst lake sediments. In this test, the null hypothesis states that there is no statistically significant difference between the samples of the different landscape units. A Mann-Whitney-Wilcox test was added for pairwise comparisons between the landscape units (Table S2).

The Mann-Whitney-Wilcoxon test was also used to test for significant differences based on the C/N (**Table S3**) and the $\delta^{13}C$ value (Table S4) between this study (Baldwin Peninsula) and other studies from Alaska: yedoma deposits along the Itkillik River (IR) (Lapointe et al., 2017; Strauss et al., 2012), DTLB deposits from the Northern Seward Peninsula (NSP) (Lenz et al., 2016) and thermokarst lake sediments from lakes in the Kobuk River Delta (KOB) and Central Seward Peninsula (CSP) (Lenz et al., 2018).

Table S2: Outcome statistical tests of bulk density (BD), total organic carbon (TOC), carbon-nitrogen (C/N) ratio and stable carbon isotopes ($\delta^{13}C$) between BAL16-B2 (yedoma), BAL16-B4 (drained thermokarst lake basin; DTLB) and BAL16-UPL1-L1 (thermokarst lake) on Baldwin Peninsula.

P-value		BD	TOC	C/N	$\delta^{13}C$
Shapiro-Wilk Test		<0.05	<0.001	<0.01	<0.001
Kruskal Wallis Test		<0.05	<0.001	<0.05	<0.001
Wilcoxon test	Yedoma – DTLB	<0.05	<0.001	<0.001	<0.001
	Yedoma – Thermokarst lake	<0.001	<0.001	<0.001	<0.001
	DTLB – Thermokarst lake	<0.001	<0.001	<0.001	<0.001

Table S3: **Outcome Mann-Whitney-Wilcoxon test of C/N ratio between yedoma, drained thermokarst lake basin (DTLB) and thermokarst lake sediments. BP: Baldwin Peninsula (this study), IT: Itkillik River (Strauss et al., 2012), NSP: Northern Seward Peninsula (Lenz et al., 2016), KOB: Kobuk River Delta and CSP: Central Seward Peninsula (Lenz et al., 2018).**

P-value C/N	DTLB BAL16-B4	Thermokarst lake BAL16-UPL1-L1	Yedoma Itkillik River	DTLB Northern Seward Peninsula	Thermokarst lake Kobuk Delta	Thermokarst lake Central Seward Peninsula
Yedoma BAL16-B2	<0.001	<0.001	>0.05	<0.001	<0.001	<0.001
DTLB BAL16-B4		<0.01	<0.001	<0.01	>0.05	<0.001
Thermokarst lake BAL16-UPL1-L1			<0.001	<0.001	<0.001	>0.05
Yedoma Itkillik River				<0.001	<0.001	<0.001
DTLB Northern Seward Peninsula					<0.001	<0.001
Thermokarst lake Kobuk Peninsula						<0.01

Table S4: Outcome Mann-Whitney-Wilcoxon test of $\delta^{13}C$ between yedoma, drained thermokarst lake basin (DTLB) and thermokarst lake sediments. BP: Baldwin Peninsula (this study), IT: Itkillik River (Strauss et al., 2012), NSP: Northern Seward Peninsula (Lenz et al., 2016), KOB: Kobuk River Delta and CSP: Central Seward Peninsula (Lenz et al., 2018).

P-value $\delta^{13}C$	DTLB BAL16-B4	Thermokarst lake BAL16-UPL1-L1	Yedoma Itkillik River	DTLB Northern Seward Peninsula	Thermokarst lake Kobuk Delta	Thermokarst lake Central Seward Peninsula
Yedoma BAL16-B2	<0.001	<0.001	>0.05	<0.001	<0.001	<0.001
DTLB BAL16-B4		<0.001	<0.001	>0.05	<0.001	<0.001
Thermokarst lake BAL16-UPL1-L2			<0.001	<0.001	<0.01	>0.05
Yedoma Itkillik River				<0.001	<0.001	<0.001
DTLB Northern Seward Peninsula					<0.001	<0.001
Thermokarst lake Kobuk Delta						<0.01

3 Supporting references

Blott, S. J. and Pye, K.: GRADISTAT: a grain size distribution and statistics package for the analysis of unconsolidated sediments, Earth Surf. Process. Landf., 26(11), 1237–1248, doi:10.1002/esp.261, 2001.

Dirghangi, S. S., Pagani, M., Hren, M. T. and Tipple, B. J.: Distribution of glycerol dialkyl glycerol tetraethers in soils from two environmental transects in the USA, Org. Geochem., 59, 49–60, doi:https://doi.org/10.1016/j.orggeochem.2013.03.009, 2013.

Hopmans, E. C., Weijers, J. W. H., Schefuß, E., Herfort, L., Damsté, J. S. S. and Schouten, S.: A novel proxy for terrestrial organic matter in sediments based on branched and isoprenoid tetraether lipids, Earth Planet. Sci. Lett., 224(1), 107–116, doi:https://doi.org/10.1016/j.epsl.2004.05.012, 2004.

Lapointe, L. E., Talbot, J., Fortier, D., Fréchette, B., Strauss, J., Kanevskiy, M. and Shur, Y.: Middle to late Wisconsinan climate and ecological changes in northern Alaska: Evidences from the Itkillik River Yedoma, Palaeogeogr. Palaeoclimatol. Palaeoecol., 485, 906–916, doi:https://doi.org/10.1016/j.palaeo.2017.08.006, 2017.

Lenz, J., Grosse, G., Jones, B. M., Walter Anthony, K. M., Bobrov, A., Wulf, S. and Wetterich, S.: Mid-Wisconsin to Holocene Permafrost and Landscape Dynamics based on a Drained Lake Basin Core from the Northern Seward Peninsula, Northwest Alaska, Permafr. Periglac. Process., 27(1), 56–75, doi:10.1002/ppp.1848, 2016.

Lenz, J., Jones, B. M., Fuchs, M. and Grosse, G.: C/N and d13C data from short sediment cores from 9 lakes in Western Alaska, [online] Available from: https://doi.pangaea.de/10.1594/PANGAEA.887848, 2018.

Peterse, F., Meer, J. van der, Schouten, S., Weijers, J. W. H., Fierer, N., Jackson, R. B., Kim, J.-H. and Damsté, J. S. S.: Revised calibration of the MBT–CBT paleotemperature proxy based on branched tetraether membrane lipids in surface soils, Geochim. Cosmochim. Acta, 96, 215–229, doi:https://doi.org/10.1016/j.gca.2012.08.011, 2012.

Peterse, F., Vonk, J. E., Holmes, R. M., Giosan, L., Zimov, N. and Eglinton, T. I.: Branched glycerol dialkyl glycerol tetraethers in Arctic lake sediments: Sources and implications for paleothermometry at high latitudes, J. Geophys. Res. Biogeosciences, 119(8), 1738–1754, doi:10.1002/2014JG002639, 2014.

Strauss, J., Schirrmeister, L., Wetterich, S., Borchers, A. and Davydov, S. P.: Grain-size properties and organic-carbon stock of Yedoma Ice Complex permafrost from the Kolyma lowland, northeastern Siberia, Glob. Biogeochem. Cycles, 26(3), doi:10.1029/2011GB004104, 2012.

Weijers, J. W.: Soil-derived branched tetraether membrane lipids in marine sediments: reconstruction of past continental climate and soil organic matter fluxes to the ocean, UU Dept. of Earth Sciences., 2007.